Graduate Theses and Dissertations                                    Graduate School

10-4-2010

# Small Antennas Design for 2.4 GHz Applications

Ibrahim Turki Nassar
*University of South Florida*

Follow this and additional works at: http://scholarcommons.usf.edu/etd

Part of the American Studies Commons

Small Antennas Design for 2.4 GHz Applications

by

Ibrahim Turki Nassar

A thesis submitted in partial fulfillment
of the requirements for the degree of
Master of Science in Electrical Engineering
Department of Electrical Engineering
College of Engineering
University of South Florida

Major Professor: Thomas M. Weller, Ph.D.
Jing Wang, Ph.D.
Gokhan Mumcu, Ph.D.

Date of Approval
October 4, 2010

Keywords: balanced, 3D dipole antenna, ground plane, meandered line antenna, Wheeler
Cap method

## DEDICATION

To my father Dr. Turki Nassar for being the best father

role model and building a highly educated family.

To my mother Rasmieh Nassar

for her encouragement, prayers, and belief in me.

# ACKNOWLEDGEMENTS

# TABLE OF CONTENTS

# LIST OF TABLES

# LIST OF FIGURES

**ABSTRACT**

In many wireless devices, antennas occupy the majority of the overall size. As compact device sizes become a greater focus in industry, the demand for small antennas escalates. In this thesis, detailed investigations on the design of a planar meandered line antenna with truncated ground plane and 3D dipole antenna at 2.4 GHz (ISM band) are presented. The primary goal of this research is to develop small, low coast, and low profile antennas for wireless sensor applications. The planar meandered line antenna was designed based on a study of different miniaturization techniques and a study of the ground plane effect. The study of the ground plane effect proved that it has a pivotal role on balancing the antenna current. The study of the miniaturization process proved that it affects directly the gain, bandwidth, and efficiency. The antenna efficiency and gain were improved using the truncated ground plane. This antenna has a measured gain of -0.86 dBi and measured efficiency of 49.7%, making it one of the efficient and high gain small antennas. The 3D dipole antenna was designed using a novel method for efficiently exploiting the available volume. This method consists of fabricating the dipole on a cube configuration with opening up the internal volume for other uses. This antenna was tested, and it was found that this antenna has good radiation characteristics according to its occupied volume. $K$a of this antenna is 0.55, its measured gain is 1.69 dBi with 64.2% measured efficiency. Therefore, this design is very promising in low-power sensing

applications. A Wheeler Cap was designed for measuring the efficiency and the 3-antenna method was used for measuring the designed antennas gain.

# CHAPTER 1

## INTRODUCTION

1.1 Background

It is expected that distributed wireless sensor networks will undergo continuous growth in the future with numerous applications such as environmental and biomedical monitoring. The design challenges in such applications differ from other modern wireless communication systems in that power consumption and size of the sensor node are the critical issues [1]. Embedding sensor nodes into objects or surrounding environments often requires small volume solutions and this introduces design challenges.

These size constraints place strict requirements on the communication system; the system frequency should be high in order to minimize the antenna size and thus the sensor node [1]. However, the path loss and DC power consumption increase with frequency; therefore, the antenna should have as high gain as possible [1]. Utilizing a high gain antenna may also be beneficial in minimizing the effect of unwanted signals from the surrounding environment. Usually a large number of sensor nodes is required in any network, therefore all the components including the antenna should have low cost.

Antennas in wireless sensor systems are one of the most critical elements that can either enhance or constrain system performance. Depending on the system application

antennas for sensor systems can be directional or omni-directional [2]. Directional antennas have the advantage of reducing the effects of interference and in extending the communication range of the system; however, the coverage area is limited. Using omni-directional antennas enables coverage of all the directions equally, therefore, they are highly preferred because usually the network nodes are randomly deployed and can be moving [1]. However, the communication range will be shorter and more likely undesired signals could be picked up.

As the transmitted power is low, efficient antennas are required for achieving successful transmission and reception of data between the sensor nodes. Due to the miniaturization of the sensor node scale and the shrinkage in volume and the limitations imposed on the antenna size, the radiation efficiency often becomes a limiting factor in overall performance of a transceiver system. This creates substantial challenges in the design of the antennas especially for embedded applications.

The impact of the surrounding space mainly influences the antenna impedance and its resonant frequency, since the electromagnetic coupling between the antenna and the surrounding medium is affected by the dielectric properties of that medium. For an antenna embedded in concrete, the relative permittivity is in the same range as that of common RF substrates where planar antennas are often fabricated, making the situation less critical than the other applications such as bio-medical sensing; here the relative permittivity values have a wide range varying with the frequency of operation. Reducing the influence of the surrounding medium is commonly achieved through the introduction of a thin dielectric coating above the antenna; this approach has proven to be successful even in the bio-medical applications [3].

The objective of this research is to advance design techniques for conformal antennas that will be integrated with a frequency multiplier, for wireless sensor nodes that are targeted for deeply-embedded and through-life structural health monitoring of civil infrastructures. Therefore, this thesis concentrates on producing simple, low cost, and conformal antenna designs that are directly integrated onto the structural packaging, and understanding the difficulties and the design restrictions that might be faced in integrating the antennas with the other components.

1.2 Thesis Organization

Chapters one and five of this thesis correspond to the introduction and conclusion, respectively, and chapters two through four describe the main focus of this work, small antenna design.

Chapter two introduces a brief examination of important antenna parameters and characteristics that should be considered in order to find an optimal design for a particular application. Additionally, a discussion of the fundamental limitations in electrically small antennas is presented, since an appreciation of these limitations has proved helpful in arriving at practical designs. Moreover, some considerations in measuring electrically small antennas and two methods for measuring the efficiency are presented, the gain/directivity method and the Wheeler Cap method, in order to determine the characteristics of the proposed antennas.

Chapter three describes the design and implementation of a planar meandered line antenna; beginning with a background theory where the miniaturization techniques, challenges, and their effects on the antenna characteristics are presented. Next, the

ground plane effect on small antennas is studied extensively. Also, a detailed explanation of the antenna design is presented, indicating one of the common problems in designing small antennas which is having an unbalanced antenna structure. Determining the gain and efficiency of the proposed antenna through measurements is then described.

Chapter four presents a study for designing and implementing a 3D dipole antenna using a novel method for efficiently exploiting the available volume. The study started with a background theory about the radiation mechanism of dipoles and the transition between unbalanced to balanced structures using a parallel plate balun. Next, detailed procedures for designing this 3D antenna and fabrication are presented.

Chapter five is the final chapter, which concludes with a summary of the findings of this research as well as recommendations for future work.

1.3 Contribution

The main contribution from this work is presenting small and low cost antenna designs, which will be directly integrated onto a structural sensor package. Specifically, the presented designs are low profile and exhibit good efficiency that is required to enhance the system performance.

A planar meandered line antenna and a 3D dipole antenna are designed, meeting the performance specifications and adding valuable studies on designing small antennas. The simulation of these devices, their characteristics, and the fabrication process have yielded an understanding of the limitation for each design and its integration capability with the wireless sensor package.

# CHAPTER 2

## SMALL ANTENNA ANALYSIS AND MEASUREMENTS

2.1 Introduction

An antenna can be defined as a transducer that can transmit or receive electromagnetic waves. Antennas can also be viewed as devices that convert between circuit power and radiated power carried in an electromagnetic wave. Antennas are usually reciprocal devices, as they have the same radiation characteristics for receiving as for transmitting.

Small is a relative term, demanding the existence of a reference standard for comparison sake. Additionally, it is critical that there must be discrimination between the physical size and the electrical size of the antenna. The scale of interest for electrical engineers dealing within the realm of wireless technologies is the free space wavelength at the operating frequency. Generally speaking, an antenna is considered to be electrically small if it fits inside the radiansphere [4]; which is the boundary between the near field and the far field of a small antenna, and its radius is one radianlength ($\lambda/2\pi$).

Most antennas would be sized at the resonant length or resonant size (multiples of $\lambda/4$) if there are no size constraints [5], since the terminal impedance of the antenna is real and easily matched with the radio or transmission line which is connected to it. Minimizing the antenna size is of interest for many wireless communication devices;

however, minimizing the antenna size is subjected to limitations, which affect directly the antenna characteristics.

In this chapter, a brief examination of important antenna parameters and characteristics will be conducted in order to find an optimal design for a particular application. Additionally, a discussion of the fundamental limitations in electrically small antennas will be presented, since an appreciation of these limitations has proved helpful in arriving at practical designs. Finally, some considerations in electrically small antenna measurements are presented and two methods for measuring the efficiency, which is one of the most important parameters in antenna design, were studied; the gain/directivity method and the Wheeler Cap method.

2.2 Fundamental Antenna Parameters

In order to find the proper antenna for a specific application several critical characteristics should be determined and specified. Antenna performance consists primarily of two aspects, the radiation properties and the impedance [6]. The radiation properties are defined by the antenna radiation pattern, gain, directivity, and polarization. The antenna impedance is related to the transfer of power from a source to the antenna when it is used as a transmitter or from the antenna to the load when it is used as a receiver [6]; therefore, the antenna should be properly matched to the transmission line connected to its terminal to avoid reflection.

The antenna radiation pattern is the directional function characterizing the radiation from the antenna, or it can also be defined as a 3D plot of the radiation in the far field region [6]. The far field distance is defined as follows:

$$R_{farfield} = \frac{2(D)^2}{\lambda}, \quad \lambda = \frac{c}{f} \tag{2.1}$$

Where $D$ is the largest dimension of the antenna, $\lambda$ is the free space wavelength, $c$ is the speed of light in free space, and $f$ is the operating frequency.

The radiation pattern is usually characterized in two dimensional plots, the elevation pattern and the azimuth pattern. Furthermore, antennas can be generally classified relative to their radiation characteristics as omni-directional or directive antennas. Well-known examples of omni-directional antennas are the microstrip patch and dipole antennas. The radiation patterns are the same for transmission as for reception for most antennas, due to their reciprocity characteristic.

Antenna directivity is a figure of merit for an antenna, which is a measure of the concentration of the radiated power in a given direction. As it is a dimensionless ratio of powers, it usually is expressed in decibels. The general expression for the directivity of an antenna is as expressed below:

$$D(\theta,\Phi) = 4\pi \frac{F(\theta,\Phi)}{\int_0^{2\pi} \int_0^{\pi} F(\theta,\Phi)Sin(\theta)d\theta d\Phi}, \tag{2.2}$$

Where $F(\theta,\Phi)$ is the radiation intensity function.

In most cases, directive antennas have considerably more gain than omni-directional antennas.

Antenna directivity gain, or gain, is a measure that depends on the efficiency of the antenna and its directional properties [7]. The gain is typically measured relative to a reference antenna (isotropic antenna) [7], and accounted for in units of dBi. The gain is

usually measured at the angle where the maximum radiation occurs [7]. The ratio of the radiation intensity in a given direction to the radiation intensity in all directions is the absolute gain [7], since the radiation intensity gives the variation in radiated power according to the position around the antenna [7]. The general equation for the directivity gain is as expressed below:

$$\text{Gain} = 4\pi \frac{F(\theta, \Phi)}{P_{in}},$$

(2.3)

Where $P_{in}$ is the total input power

One of the most important antenna parameters is the efficiency, which is defined as the ratio between radiated power and input power. The total antenna efficiency accounts for all the losses, at the input terminal and within the antenna structure, which include the conduction, dielectric, and surface wave losses, as well as reflection loss [7]. The reflection efficiency $\in_r$ can be described as a result of the reflection due to the mismatch at the antenna input terminal, between the antenna and the transmission feed line, and it is given by the following formula:

$$\in_r = 1 - \Gamma^2,$$

(2.4)

Where

$$\Gamma = \frac{Z_{in} - Z_o}{Z_{in} + Z_o}$$

The overall efficiency is given by

$$\in_o = \in_c \in_d \in_r,$$

(2.5)

8

Where $Z_o$ is the reference impedance of the source, $Z_{in}$ is the input impedance of the antenna, $\epsilon_r$ is the reflection efficiency, $\epsilon_c$ is the conduction efficiency, and $\epsilon_d$ is the dielectric efficiency.

The conduction-dielectric efficiency $\epsilon_{cd}$, which is known as the radiation efficiency, is defined as the ratio between the radiated power to the accepted power, which can be expressed in terms of the radiation resistance and the loss resistance as follows:

$$\epsilon_{cd} = \frac{R_r}{R_l + R_r},$$  (2.6)

Gain and directivity are related also by the radiation efficiency, since the gain accounts for the antenna losses; therefore, the radiation efficiency can be defined as follows:

$$\epsilon_{cd} = \frac{Gain}{Directivity},$$  (2.7)

Calculation of losses is difficult, thus, measurement is often the only way to reliably determine the antenna efficiency [8]. This measurement will be discussed more in depth in section 2.5.

Polarization is the orientation of the transmitted or received electric field in the far field in a given direction. The instantaneous E-field of a plane wave traveling in the z direction can be expressed as, [7]:

$$\overline{E}(z;t) = Ex(z;t)\overline{x} + Ey(z;t)\overline{y},$$  (2.8)

According to the above equation, the polarization can be classified as linear where the electric or magnetic vector field is always oriented along a line [7]. The other two classes

9

of polarization are circular polarization, where the electric field vector traces a circle as a function of time [7], and elliptical polarization which occurs if the field vector traces an ellipse in the far field [7]. For better performance, the polarizations of the transmitting antenna and the receiving antenna must be matched to reduce the polarization loss factor. This factor is very important in the gain and radiation pattern measurements, since the power received by an antenna will be reduced if there is a polarization loss. As the E-field vector is always parallel to the electric current vector, the polarization can in some cases be easily determined by knowing the antenna current direction.

Many times, the bandwidth (BW) of an antenna is not clearly defined; therefore the quality factor (Q) has more interest. Q is usually expressed in terms of the voltage standing ratio (VSWR) or related to the return loss at the input terminals. In general, the bandwidth can be defined as the range of frequencies where the antenna characteristics are meeting the desired application requirements.

2.3 Fundamental Limitations on Electrically Small Antennas

Electrically small antennas are antennas smaller than the radian sphere, which is the boundary between the near field and the far field, with a radius at $\lambda/2\pi$, as defined by Wheeler [4]. The configuration described by Wheeler is illustrated in Figure 2.1.
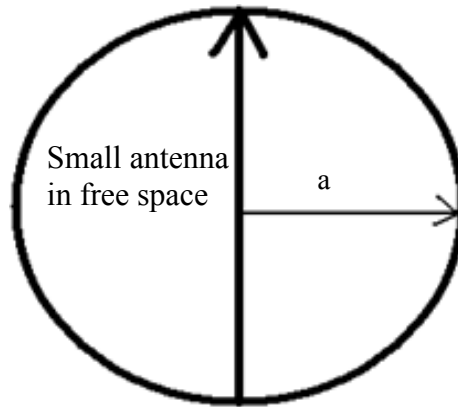
Figure 2.1: Antenna within a Sphere of Radius a

The small antenna is enclosed in a sphere of radius $a$ in free space, where $a$ is the radius of the smallest sphere that can enclose the antenna. This relationship can be expressed as below:

$$ka < 1, \qquad\qquad (2.9)$$

Where k=$2\pi/\lambda$ (radians/meter)

$\lambda$ = free space wavelength (meters)

$a$ = radius of sphere enclosing the maximum dimension of the antenna (meters)

Such small antennas are subject to limitations. An antenna within this limit of size behaves fundamentally as lumped capacitance or inductance [9], however, if the small antenna is free of loss it could receive and transmit an amount of power independent of its size [9]. This requires that the antenna be resonated at one resonant frequency and without adding any losses [9]. As the small antenna radiation resistance is governed by physical laws, the antenna radiation resistance decreases significantly with the antenna size. In some cases the small antenna loss resistance may be higher than the radiation resistance. Therefore, minimizing the antenna size within acceptable performance is governed by fundamental limits.

11

The fundamental limits on how a small antenna can be made have been studied by several authors. Wheeler defined the radiation power factor and calculated the maximum power factor achievable by an antenna to quantify the radiation efficiency; because of the small size this factor is always less than one [9]. The radiation power factor is computed from the radiation resistance or conductance, and it is proportional to the volume of the radiansphere and a shape factor [10]. A reasonable approach to increase the radiation power factor is by exploiting the sphere volume effectively [10], if the antenna is limited by a maximum dimension not by an occupied volume.

Chu subsequently generalized Wheeler's work by considering the fields outside the smallest possible sphere circumscribing the antenna in order to find the radiation quality factor (Q) of an antenna, which is an important factor related to the small antenna performance. The external fields to the sphere surrounding an antenna, due to an arbitrary current inside the sphere, are represented by spherical wave functions, called modes [11]. These modes deliver power independently from each other [12]. By expanding the spherical wave function, the radiation Q can be calculated in terms of the radiated power and the non-propagating energy external to the sphere [12], thus this radiation Q will be the minimum possible radiation Q for any antenna that can be enclosed by that sphere [11]. As with any propagating wave, the total time average stored energy outside the sphere is infinite, thus, calculating the radiation Q is complicated [12]. Therefore, to separate the energy associated with radiation, Chu reduced the field problem to a circuit problem, where the radiation loss is replaced by an equivalent conduction loss. An equivalent ladder network was derived for each spherical waveguide mode [12]. In addition, the conduction loss was neglected to simplify the problem.

Hansen used the same concept of the smallest sphere that encloses the small antenna, and mentioned that higher order modes may not be present for $ka < 1$. Through his work, Hansen derived the following approximate formula for Q [13]:

$$Q = \frac{1+3(ka)^2}{(ka)^3[1+(ka)^2]},$$ (2.10)

which shows that Q varies inversely with the cube of the radius of the sphere.

Typically antennas are not self-resonant; therefore, the radiation Q of such an antenna is ambiguously defined [12]. In general, the radiation quality factor can be defined, as an ordinary circuit element, to be $2\pi$ times the ratio of the maximum energy stored to the total energy lost per period [12]. Harrington [14] derived the following expression for the radiation Q of an ideal loss-free antenna:

$$Q = \begin{cases} 2w \dfrac{W^{elec}}{Re(P)} & W^{elec} > W^{mag} \\[4mm] 2w \dfrac{W^{mag}}{Re(P)} & W^{elec} < W^{mag} \end{cases}, (2.11)$$

where $W^{elec}$ is the time average non-propagating stored electric energy, and $W^{mag}$ is the time average non-propagating stored magnetic energy, and $w$ is the radian frequency, and Re(P) denotes the radiated power.

Mclean reexamined the Chu derivation and Hansen's approximate expression for Q, and based on the Harrington definition for the radiation Q above, derived the following exact expression for the minimum radiation Q ($Q_l$) for a linearly polarized antenna:

$$Q_l = \frac{1}{(ka)^3} + \frac{1}{ka}, \tag{2.12}$$

Also he derived the minimum Q for circularly polarized antennas, which is expressed as:

$$Q_l = \frac{1}{2}\left(\frac{1}{(ka)^3} + \frac{2}{ka}\right), \tag{2.13}$$

For very small antennas, it can be noticed that the above two expressions for the quality factor become similar, and agree with the other expressions from the other authors. Figure 2.2 shows a graph of the minimum radiation Q for a linearly polarized antenna in free space, based on eq. 2.12.
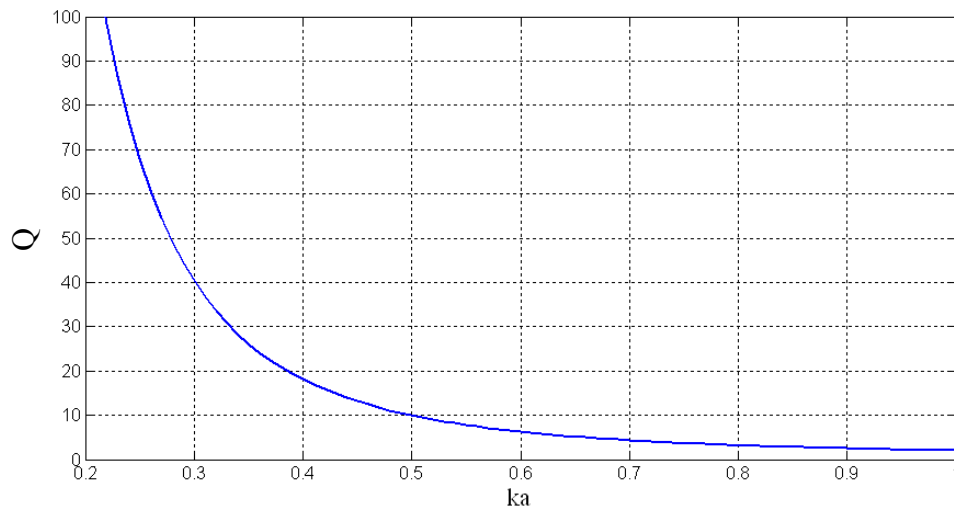


Figure 2.2: The Minimum Radiation Quality Factor for a Linearly Polarized Antenna

As seen in Figure 2.2, as the volume shrinks, the quality factor increases rapidly, therefore the bandwidth decreases; this is attributed to the strong reactive part of the antenna impedance. High Q factor is a problem in most of the communication systems, since impedance matching becomes difficult and the bandwidth is very narrow. Moreover, a smaller antenna with the same impedance requires more effort in tuning in order to deliver its available power [9].

14

Sten et al. evaluated the limits on the fundamental Q of a small antenna near a ground plane, and found that it depends on the radius of the smallest sphere that encloses the antenna and its image [15]. Horizontal and vertical electrically small antennas over a large ground plane have different Qs; for the vertical case, it is found that Q is equivalent to the free space case [16], however for a horizontal electrically small antenna near a large ground plane, the Q becomes large and the bandwidth becomes small [15]. As the separation distance between a horizontal electrically small antenna and a conductor surface decreases, the radiation efficiency decreases and the stored near field energy increases, since the tangential electric field component vanishes [16].

Recently Best defined the small antenna as one with $ka < 0.5$, and found that the quality factor of an electrically small wire antenna is primarily determined by the antenna's height and effective volume [17]. Therefore, the small antenna volume must be utilized in radiation for the purpose of achieving the best compromise between the bandwidth and the efficiency [18].

The relation between the radiation Q and the maximum achievable bandwidth is not direct; however, in general as the radiation Q increases the maximum achievable bandwidth decreases [12]. An approximate expression of the bandwidth for an RLC circuit type in terms of Q is as expressed below [16]:

$$BW = \frac{S-1}{Q\sqrt{S}},$$ 
(2.14)

where $S$ is the voltage standing wave ratio and BW is the normalized bandwidth.

The gain that a small antenna can have is also governed by physical laws. Harrington gave a practical upper limit for the gain that an antenna can achieve, which is defined as the maximum gain obtainable using wave functions of order $n \leq N = \beta R$, where $\beta R$ is identical to $ka$ and $n$ is an integer number [14]:

$$G = (\beta R)^2 + 2\beta R, \tag{2.15}$$

This formula is valid for antennas with $ka > 1$, to satisfy the assumption of having at least one propagating mode. Harrington has stated that antennas can have a higher gain than this limit, in which case they are classified as super gain antennas. According to Harrington's definition, small antennas are super gain antennas as it is possible for a small antenna to have a gain above this limit, such as a short dipole antenna. However, the bandwidth will be narrow and the losses will be high because of the high field intensities at the antenna structure [14]. Figure 2.3 illustrates a graphical form of Harrington's upper gain limit for an electrically small antenna with respect to $ka$.
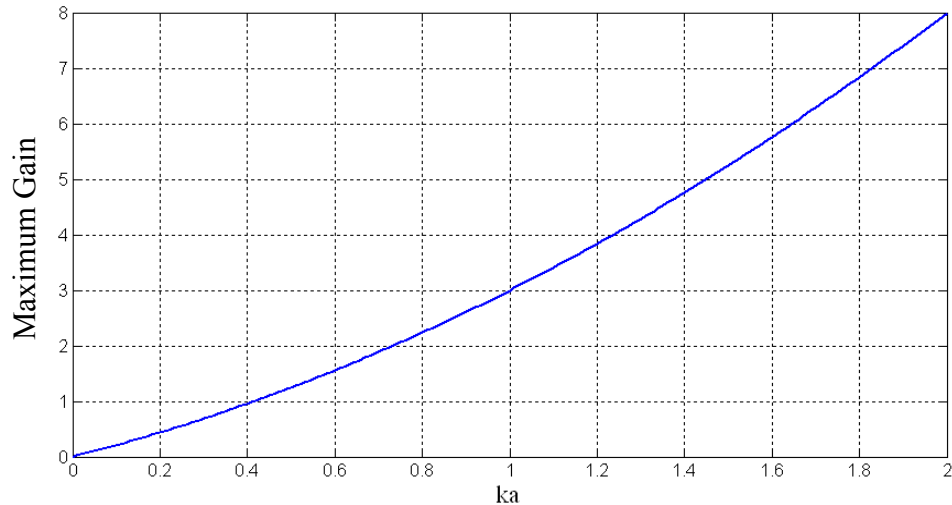


Figure 2.3: Harrington's Upper Gain Limit

16

As seen in Figure 2.3, the upper gain limit of an antenna with $ka = 1$ is 3. It is widely accepted to consider the maximum linear gain of a small antenna with $ka < 1$ to be 3 independent of its size, which is similar to the maximum directivity that a small antenna can achieve.

The maximum directivity of a single port small antenna is the same as that of Huygen's source, which has a directivity of 4.8 dBi [19]. Small antennas that have a small ground plane can have a directivity that approaches this limit [19], and small antennas that have large ground planes can have directivity higher than the maximum limit. However, if the ground plane size is included in the definition of the smallest sphere, the directivity may not approach the limit [19].

The following reasonable formula can be used to find the maximum directivity at all antenna sizes, [19]:

$$D_{max} = (ka)^2 + 3,$$
(2.16)

Figure 2.4 illustrates how the directivity can be increased by increasing the antenna size.
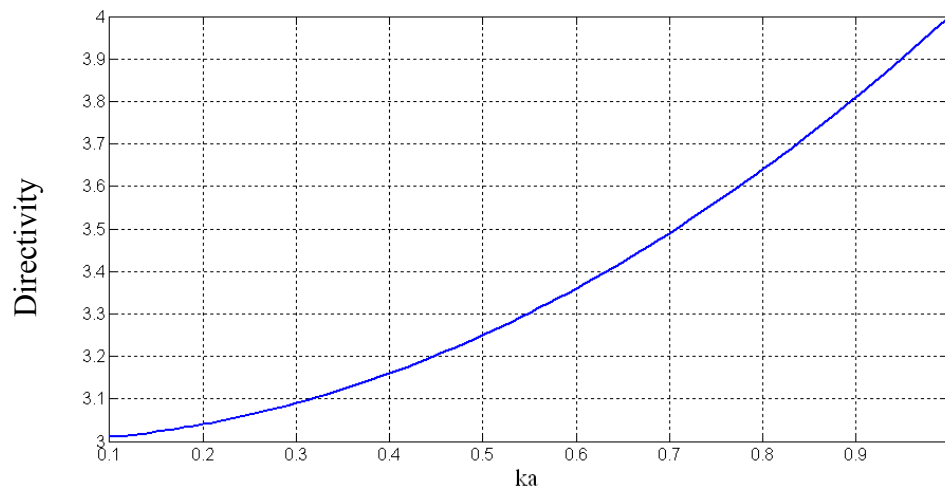


Figure 2.4: The Maximum Antenna Directivity

As seen in the above equation, as the small antenna size (*ka*) decreases, the directivity remains approximately constant, therefore they can be classified as super directive antennas [20].

Small antennas usually have omni-directional patterns (doughnut shaped) of a Hertzian dipole of directivity of 1.5. However, by applying different electric and magnetic Hertzian dipole arrangements other patterns are possible with a directivity ranging approximately from 1.5 to 3 [20].

2.4 Electrically Small Antenna Measurement Considerations

As the available space for antennas decreases until the structure defined as "the antenna" is small electrically and physically, it will be inaccurate to consider just that part of the overall wireless device structure in the measurements [21]. Therefore, measuring electrically small antennas is challenging and prone to errors.

The antenna feed structure plays an essential role in the errors that may be faced in such a measurement. Usually a coaxial feed cable is part of the feed network. The coaxial feed cable current is one of the main reasons for obtaining inaccurate results. If the antenna is balanced, a balun needs to be used as a transition between the unbalanced feed cable and the balanced radiator. If the balun is not designed properly and the antenna is not well-matched, a large part of the antenna reflected signal will reside on the coaxial feed cable outer conductor [21]. As a result, the input impedance measurement will be inaccurate, usually indicating better match than is correct [21], and the measurement will be unrepeatable, as the measurement is sensitive to the cable position and moving one's hand along the cable (for example).

The cable current also affects the gain, efficiency, and radiation pattern measurements. Assuming a dipole antenna (which is balanced) is connected directly to unbalanced feed (such as coaxial cable), a high current distribution residing on the cable will be observed. This current will radiate along with the antenna, creating errors in the measurements and usually indicating, higher gain, higher efficiency, and perfect omni-directional patterns [21]. This current will also alleviate the null and reduce the cross polar discrimination of the dipole [22]. Therefore, measuring the radiation patterns is a good approach to observe the cable current radiation effect.

In order to measure the input impedance and the radiation patterns correctly, a choke could be used, as discussed in [21]. There are different versions of these chokes, as presented in [23], however, usually they are appropriate for an operating frequency below 1 GHz. Another option is the implementation of an optics based system to reduce the cable currents, which is described in [24]. Usually a balun needs to be used, and it becomes part of the design.

The increasing push for small antennas concurrently leads to a push for small ground planes, until the antenna performance becomes strongly dependent on the ground plane size [21]. When an electrically small structure is placed over a larger conducting structure (as with many monopole antennas) the ground plane usually will be the main radiating source [21]. For an unbalanced antenna the ground plane needs to be large enough to provide the necessary image currents—more discussion about the ground plane effects will be presented in section 3.3. A ground plane that circular rather than rectangular, with a diameter larger than about 1.25 wavelengths tends to give reasonable impedance and radiation characteristics [21].

2.5 Efficiency and Gain Measurement Methods

Efficiency, an important parameter in antenna performance, is often difficult to quantify correctly [8]. Many factors can reduce the efficiency considerably, including the antenna feed network losses and surface wave excitation. It was found in [8] that by theoretical calculations these losses can be estimated, however, some factors such as surface roughness and spurious radiation, cannot be estimated by calculation. Therefore, in many cases the only way to reliably determine the antenna efficiency is through measurement. Two methods were studied for measuring the efficiency, the gain/directivity method and the Wheeler Cap method.

2.5.1   Gain/Directivity Method

The most well-known way of measuring antenna efficiency is to determine the gain and the directivity of the antenna and compute the efficiency as in the following formula:

$$efficiency = \frac{gain}{directivity},$$
(2.17)

There are some drawbacks associated with this method, which may make the resulting efficiency value inaccurate. Power radiated, power dissipated in the dielectric, power dissipated in the conductors, and power delivered to surface waves all compose the input power [8]. Also the feed network radiation and surface wave power diffraction may become part of the radiated power of the antenna. As a result, these powers may not show up as a loss in the efficiency measurement [8].

Another problem associated with the gain/directivity method is that gain and directivity are determined independently, so the technique does not account for the cancelation of errors common to the measurement of both quantities [8]. One possible solution to this problem could be by determining the directivity through integration of the measured pattern data [8].

The gain can be measured using several techniques depending on the frequency of operation [7]. Two common gain measurement methods are the absolute-gain approach which does not require a prior knowledge of the gains of the antenna, and the gain-comparison which requires standard gain antennas [7]. The antenna absolute gain can be determined by two common methods; the two antenna method, and the three antenna method. The three antenna method is employed if the antennas in the measuring system are not identical [7].

## 2.5.2   Wheeler Cap Method

The Wheeler Cap method employs a conducting shell enclosure that is used to measure the efficiency of a small antenna. Ideally, this shell is a perfectly conducting spherical shell which has an inner surface located at the radian sphere [5], Figure 2.5.

λ/2π

Small Antenna

Perfectly Conducting
Spherical Shell
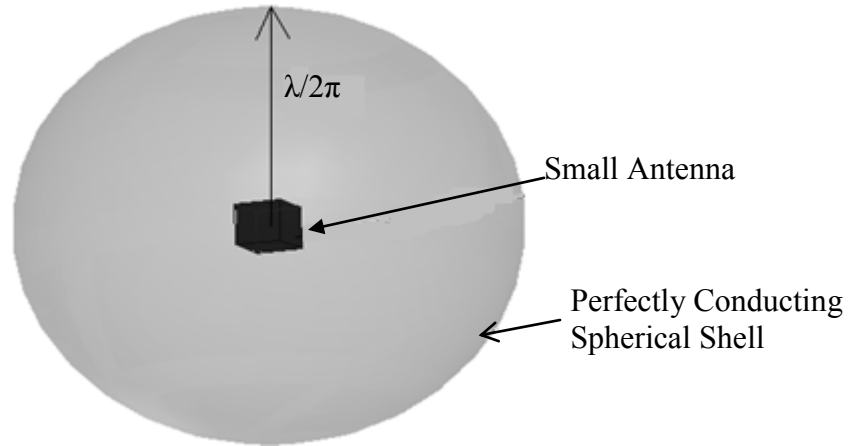
Figure 2.5: A Wheeler Cap Enclosing a Small Antenna

The purpose of the shell is to block the small antenna from radiating, so any power absorbed is a loss [5]. A simple measurement of the input impedance would then give the loss resistance. After which measuring the input impedance without the cap will give the sum of the loss resistance and the radiation resistance. These procedures are based on the assumption that the current distribution is not affected by placing the antenna inside the cap [5].

Microstrip antennas are known with their extended substrates, thus a larger Wheeler Cap is often required [25]. However, interior cavity modes can be supported by larger Wheeler Caps that may interfere with the resonant frequency of the antenna, causing errors in measuring the input impedance value [25]. A reduction in the Wheeler Cap height can be helpful in pushing these modes to higher frequencies [25]. Therefore, the Wheeler Cap height could be a critical factor in obtaining an accurate measurement.

A contradiction was found in different references relating to the Wheeler Cap size, material, and the placement of the antenna inside the cap. Wheeler mentioned that the size and shape are not critical, however, the cap must be electrically large so that the

near fields are not affected while still preventing radiation, and small so that cavity resonances are not excited. In reference [26], it is proved that it is effective to select the shield where the frequency shift is not caused, based on the fact that only the contribution of the radiation can be removed by using a very small shield. However, it was found that the effect of reducing the cap size is to increase the input reactance but, so long as accurate values of input resistance could be determined [27]. Also, it is important that the cap make good electrical contact with the ground plane, and it is necessary to have the cap perfectly centered, as moving the cap off center causes the impedance to move approximately along lines of constant resistance. However, in reference [8], it was mentioned that the size of the cap is not critical, and that the shape of the cap need not to be spherical. It was also found in [8] that the conductivity of the cap was not crucial. Therefore, it can be concluded from this contradiction that the Wheeler Cap size, material, and shape and the antenna position inside the cap can have an effect on the efficiency measurement, depending on the antenna size and type. Generally speaking, the cap needs to be a conducting shell that can enclose the antenna without causing a frequency shift and changing the current distribution on the antenna.

The efficiency is defined according to how the antenna under test behaves near its resonance. If the test antenna behaves more like a series RLC circuit near its resonance, then the input resistance R should decrease after placing the cap and the efficiency is calculated by the following formula [25]:

$$Eff = \frac{R_{nocap} - R_{cap}}{R_{nocap}},$$
(2.18)

23

If the test antenna behaves like a parallel RLC circuit near its resonance, then G at the antenna resonance should decrease after placing the antenna inside the cap, which will lead to an increase in the input resistance [25]. Therefore, the efficiency can be determined using the following expression:

$$Eff = \frac{G_{nocap} - G_{cap}}{G_{nocap}}, \qquad (2.19)$$

2.6 Conclusion

The small antenna limitations that have been studied verified that larger antennas are generally more efficient, especially for wide bandwidth applications. However, it was found that if an antenna is restricted by a maximum dimension but not by an occupied volume, the radiation power factor and the gain can be increased by exploiting the available volume.

Consequently, 3D antennas are preferred for applications that require efficiency concurrently with small size, since these antennas make more efficient use of the available volume by realizing relatively long antenna lengths. 3D antennas are also beneficial in providing additional space within the inner structure for other uses, such as storage room for batteries or other circuit elements.

Measuring an electrically small antenna is challenging and careful consideration of cable effects and ground plane size needs to be taken in order to achieve accurate and repeatable results [21]. The antenna feed structure plays a critical role in the errors that may be faced in measuring the input impedance, the resonant frequency, the radiation patterns, and the efficiency.

The gain/directivity method for measuring the efficiency is simple in principle but it was found that it lacks of repeatability and its uncertainty is relatively large [8]. In contrast, the Wheeler Cap method is the easiest to implement and gives good accuracy with repeatable results [8]. The Wheeler Cap size can have an effect on the efficiency measurement, and can become critical, depending on the size of the antenna, and its type. The position of the antenna inside the cap can have also an effect on the efficiency measurement.

# CHAPTER 3

## PLANAR MINIATURIZED ANTENNA

3.1 Introduction

Miniaturization is a continuing trend in the production of many wireless devices. In antennas there is a need to shrink the occupied volume, while at the same time maintaining acceptable radiation characteristics. The miniaturization process is governed by physical laws; therefore, miniaturization generally involves a well-balanced compromise between size, bandwidth, and efficiency.

One of the main size limitations in antenna design is the ground plane, which is the largest part of many antennas. The ground plane plays a fundamental role in the antenna characteristics, and its size affects the gain, bandwidth, input impedance, and resonant frequency. Most small antennas are unbalanced, and therefore the suitable ground plane needs to be within a specific size in order to absorb the charge flow [28], as a result this creates a greater challenge in minimizing the antenna size.

In this chapter a brief discussion of different miniaturization techniques and their effects on the antenna radiation characteristics are presented. A study of the ground plane effect is also carried out. Based on this study, a meandered line microstrip antenna was investigated; it was designed, fabricated, and measured for an operating frequency of 2.4

GHz. Good agreement was obtained between the expected and measured response for the final design. In order to improve the gain, a truncated ground plane was used.

In order to measure the efficiency of the antenna, a Wheeler Cap has been designed. The efficiency measurement was then verified using the gain/directivity method. In the gain/directivity method, the maximum gain was measured using the 3-antenna method [7], after which, the simulated directivity, using Ansoft HFSS11, was used to compute the efficiency. *Ka* of the final antenna design excluding the ground plane is 0.26, it has a gain of -0.86 dBi and an efficiency of 49.7 %, and therefore, it is one of the more efficient and high gain small antennas.

## 3.2 Miniaturization Techniques

The miniaturizing techniques that are utilized to reduce the overall size of antennas consist mainly of antennas loaded with materials, modifying the geometry, using the antenna environment, and loading the antenna with lumped elements. Each of these techniques is discussed in the following sections.

### 3.2.1 Loading with Materials

The antenna resonant frequency depends on the wavelength in the antenna structure, which is determined by the space permittivity and permeability around the metal structure. The wave length $\lambda$ is expressed as:

$$\lambda = \frac{c}{f * \sqrt{\mu * \varepsilon_{eff}}},$$
(3.1)

where $\varepsilon_{eff}$ is the effective relative dielectric constant and $\mu$ is the relative permeability.

As seen in the above equation, the wavelength is a function of the permeability and the effective dielectric constant which depends on the permittivity and the shape of the dielectric. As the dielectric constant and the space permeability increases, the wavelength becomes shorter.

Antennas are usually resonating at $\lambda/2$ and $\lambda/4$. Since the wavelength is shorter in a high permittivity substrate the antenna becomes physically smaller. However, this high dielectric loading will reduce the efficiency as the high permittivity substrate concentrates more electric field inside the substrate [18]. If there is no loss added by this loading the bandwidth will decrease and the quality factor will increase rapidly for the same reason [18].

The loading of the antenna can also be done using a thicker substrate and superstrate. A thicker substrate increases the radiation efficiency and minimizes the antenna electrical size. The superstrate has the same effect on the antenna, and an efficient way to use it is by placing it over the areas with higher current distribution [29], since this will minimize the current distribution and is a key factor in improving efficiency. High current distribution implies high energy storage and large power dissipation, therefore, low efficiency [11].

3.2.2    Modifying the Geometry

Modifying the geometry is a smart and reasonable way to minimize the antenna size. This idea came from the fact that for a minimum quality factor the antenna must exhibits maximum effective volume, when it is confined within a circumscribing sphere, as discussed in the previous chapter. A good example for this technique is the inverted *L*

28

antenna, which came from a monopole antenna by bending its length or height [18]. Other examples are the 3D antennas which will be discussed in the next chapter, and slot antennas. Slot loading shifts the resonance toward lower frequencies, and this frequency shift can be interpreted as an increase of the total capacitance of the antenna; however, this approach reduces the antenna efficiency [30]. The meandered line antennas are another example of modifying the geometry; this approach can reduce the effective antenna length, and it will be described more within the antenna design section.

Another approach of modifying the geometry is using ground planes and shorting pins, a well-known example of this approach is the quarter wave patch antenna. For a regular patch antenna operating in the TM10 mode, the length $L$ should be as in the following formula:

$$L = \frac{c}{2*f*\sqrt{\epsilon_{eff}}},$$ (3.2)

A rectangular patch antenna was designed in this work, and Figure 3.1 illustrates the patch antenna structure. As seen, $L$ is 18.5 mm for the 2.4 GHz design frequency. Figure 3.2 illustrates the simulated return loss and the resonant frequency.
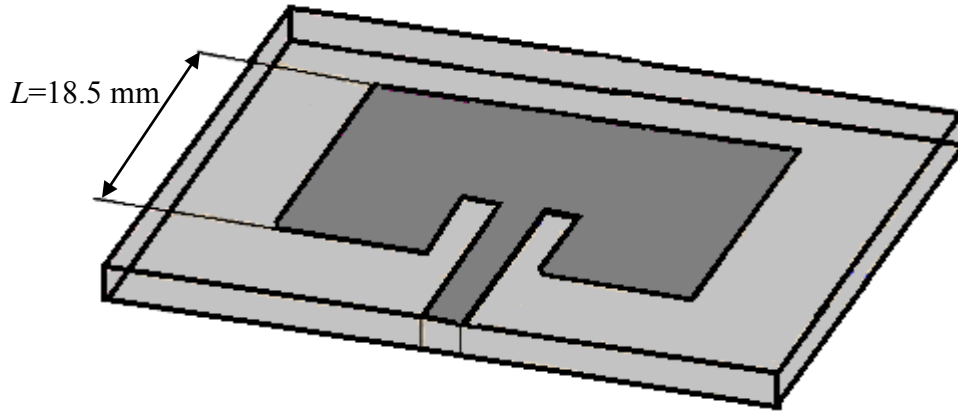
Figure 3.1: Rectangular Patch Antenna
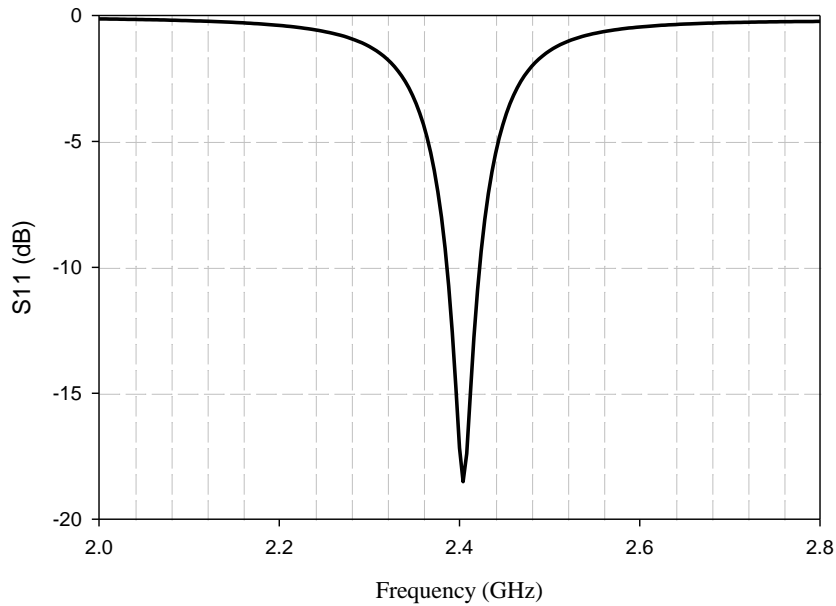


Figure 3.2: Simulated Return Loss for the Rectangular Patch Antenna

The electric field varies every $\lambda/2$ along its length, becoming zero at $L/2$. An electric wall can be used at this point to reduce the length by a factor of 2, without affecting the field distribution [31].

Instead of using a shorting wall, shorting via holes could be used. These vias can do the same job; however, they have some inductance and small resistance, which can help in matching the antenna input impedance if used properly. Also, these vias disturb

the current distribution on the ground plane, which can create unbalanced effects. Figure 3.3 and 3.4 shows the same conventional patch antenna in Figure 3.1 after adding shorting via holes of 0.8 mm diameter. As seen the length has decreased by a factor of 2.
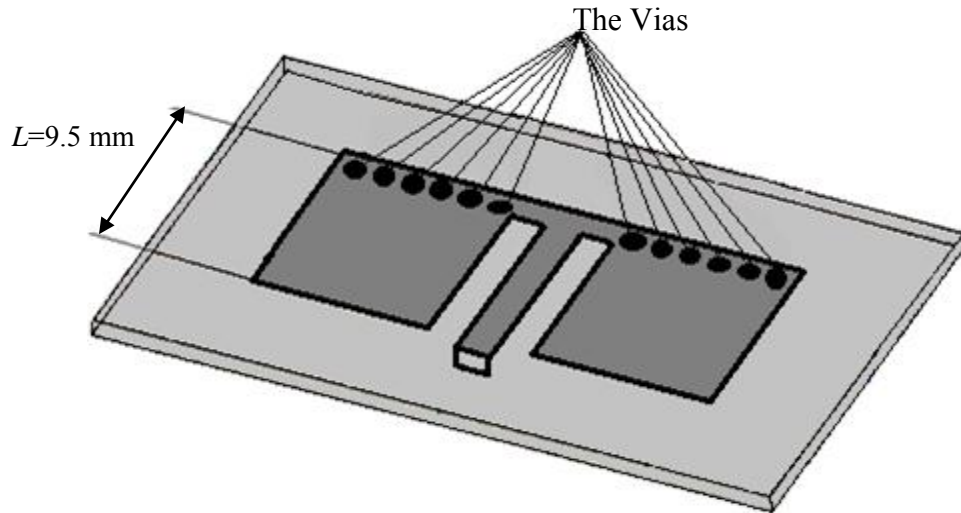


Figure 3.3: Quarter Wave Patch Antenna
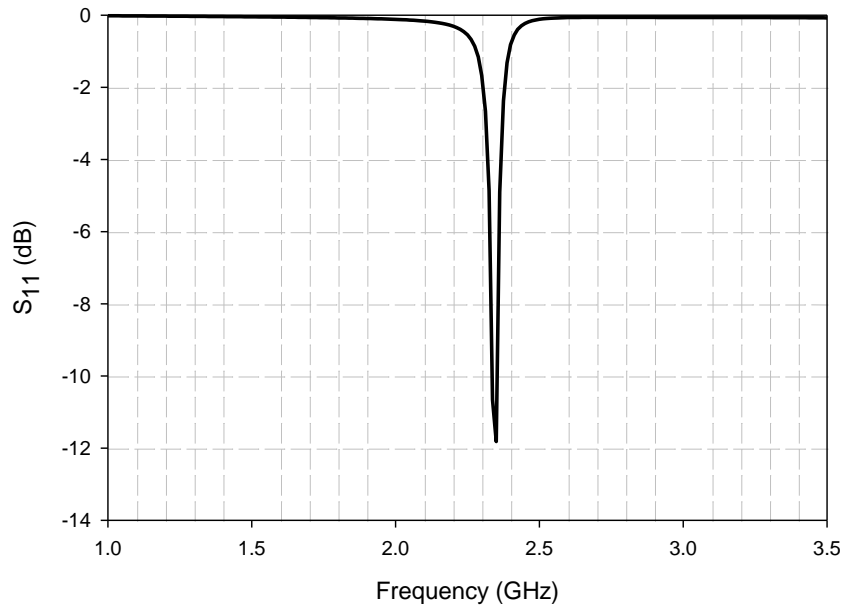


Figure 3.4: Simulated Return Loss of the Quarter Wave Patch Antenna

### 3.2.3  Using the Antenna Environment

As discussed in chapter two the efficiency will decrease in designing small antennas, therefore, a useful way to improve the radiation efficiency is by making the antenna environment participate in the radiation process [18]. The casing of an antenna can be part of this 'antenna environment' in some designs. However, in some designs the antenna may be just working as a resonator to determine the operating frequency and the casing radiates most of the power [18]. The SMILA (Smart Monobloc Integrated-L Antenna) is one of the antennas that use this technique [32]. The surrounding medium directly affects the small antenna performance; therefore, careful consideration should be taken in order to integrate these antennas into a system [18].

### 3.2.4  Loading with Lumped Elements

When an antenna becomes smaller than a half wavelength, it will have high reactive input impedance [18], which can be compensated for by lumped element loading. Loading the antenna by reactive components can make it smaller, however, if these elements have losses, this will decrease the efficiency [18].

Lumped elements can be used as a matching network to achieve a low voltage standing wave ratio at the input. With this approach there will be no need to adjust and optimize the antenna structure [33].

### 3.3 The Ground Plane Effect

The ground plane is the largest part of many antennas. Therefore, it becomes one of the main challenges in minimizing the overall antenna size. The ground plane size and

shape have a significant impact on the resonant frequency of the antenna, if it is below a certain size [34].

A finite ground plane affects the resonant frequency, and for a patch antenna with a finite ground plane size, the resonant frequency is higher compared to one with an infinite ground plane. The resonant frequency decreases and approaches that of the infinite ground plane as the size of the ground plane increases [31].

A finite ground plane also gives rise to radiation from the edges of the ground plane, therefore, changes in the radiation pattern and the directivity, as was mentioned in [31]. It was found also that the E-plane radiation pattern is affected more than the H-plane pattern by the finite sized ground plane [31], and the finite ground plane size causes ripple in the radiation pattern.

The radiation efficiency is also dependent on the ground plane size, and a compromise may be needed between desired efficiencies and a large ground plane [35]. Moreover, it was found in [34] that the gain is affected strongly by the ground plane size, and this dependence is complex, as the ground plane size increases the peak gain increases, reaching a maximum limit for an infinite ground plane.

For most monopole antennas, the impedance characteristics depend strongly on the ground plane size [36]. In general, achieving good impedance matching within the operating bandwidth requires an adequately sized ground plane, since the size of the ground plane affects the impedance at the input terminal and the resonant frequency [36].

The effect of the ground plane arises from the fact that the ground current is one of the dominant factors in determining the small antenna radiation properties and the

input impedance, and the ground plane size affects this current distribution to some limits (especially the current amplitude) [36]. However, the antenna position above the ground plane is more important [37]. For example, in F antennas the antenna should be placed close to the corner of the ground plane, where the short circuit plate is at the ground plane edge, for optimal gain and bandwidth [34]. Also, as will be mentioned in the design section, the ground plane size and position has a critical effect on balancing the current on the antenna and the feed network, since the suitable ground plane needs to be within a specific size in order to absorb the charge flow [28]. Therefore, it could be argued that in some cases the ground plane should be included in determining the antenna size or its radian sphere [37].

## 3.4 Planar Meandered Line Antenna Design

Based on the study of the miniaturization techniques, a meandered line antenna operating at 2.4 GHz was designed, fabricated, and measured. The miniaturization techniques that have been used are; antennas loaded with materials, using ground planes and short circuits, and modifying and optimizing the geometry.

The substrate material that was selected is Rogers/RT Duroid 6010 with a nominal dielectric constant ($\varepsilon_r$) of 10.2, and thickness of 100 mils. This high permittivity substrate will reduce the antenna size, as discussed in section 3.2.1, however, a higher permittivity is unfortunately often equivalent to higher dielectric losses [18].

### 3.4.1   The Initial Design

The meandered line approach was employed to minimize the antenna size. After that a shorting via hole was added to connect between the patch metallization and the

ground plane to reduce the antenna length. Since this approach gives rise to a residual inductance, the antenna length must be adjusted to account for the added inductance, which was approximately 0.7 nH. In order to match the antenna input impedance to 50 ohms, the via was placed at the input of the antenna and close to the feed point.

In order to minimize the input reactance and maximize the input resistance without degrading the efficiency, Ansoft HFSS11 has been used to optimize parameters such as: the total length of the meander line of the antenna, the location of shorting vias, the number of meandered sections, the slot size between sections, the width of the meander line, the total length and width of the structure, and the dimensions and location of the feed line. The final design and the simulated results are shown in the following figures. A lumped port was used to excite the antenna in HFSS, and the metal thickness was not included in the simulation.
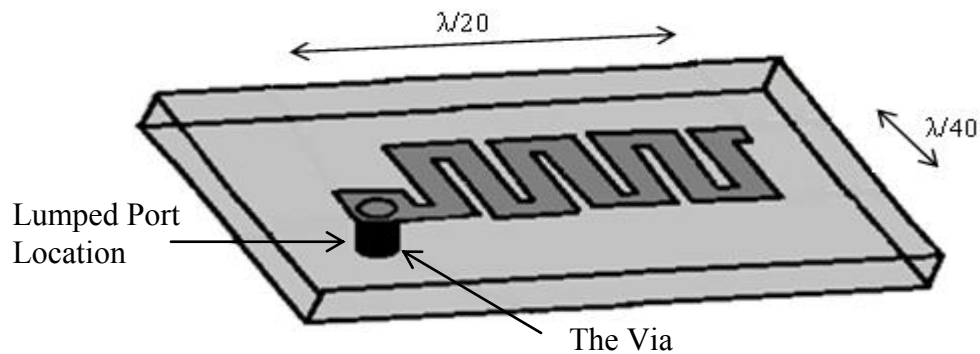


Figure 3.5: The Geometry of the Initial Meandered Antenna Design
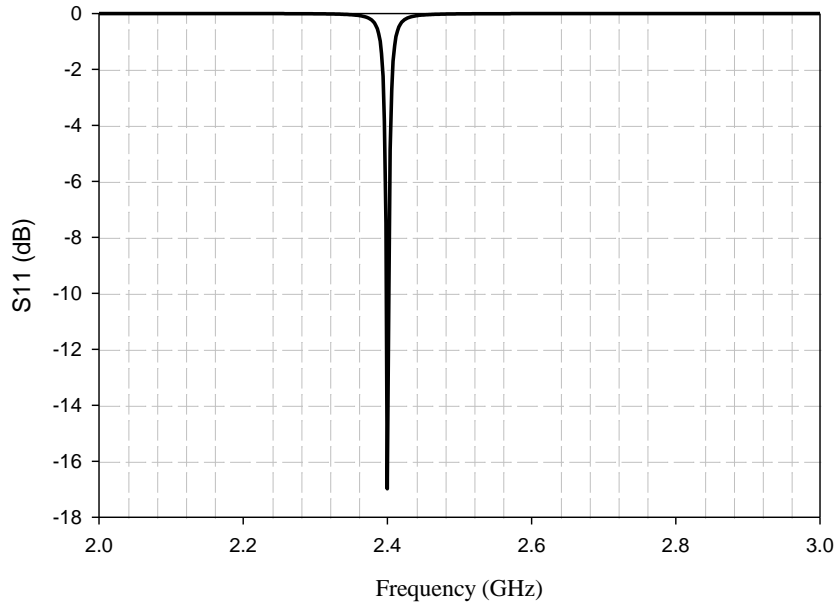
Figure 3.6: The Simulated Return Loss of the Initial Design
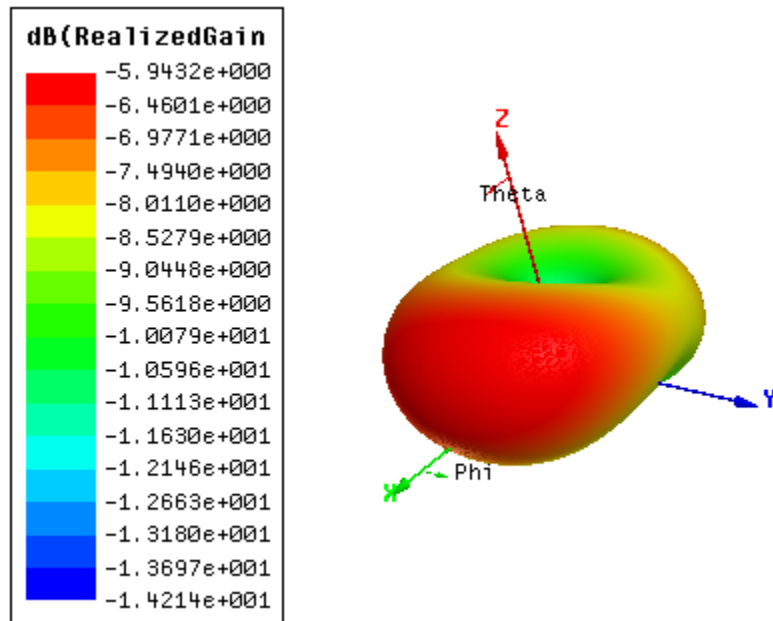


Figure 3.7: The Simulated 3D Radiation Pattern of the Initial Design

As shown in Figure 3.6 the bandwidth was very narrow (0.5%), and the radiation

pattern in Figure 3.7 is not perfectly omni-directional as there is a 3 dB difference

between the null and the peak value in the $\theta=90^{\circ}$ plane. Table 3.1 summarizes the final

simulated parameters for the initial design at 2.4 GHz.

Table.3.1: Antenna Parameters for the Initial Design

| Maximum Return loss | 16 dB |
|---|---|
| Directivity | 1.79 |
| Peak gain | 0.25 |
| Radiation Efficiency | 14% |
| Ka | 0.17 |
| 10 dB Return Loss BW | 0.5% |

The miniaturization techniques that have been used produce greater current

concentrations on the antenna, and therefore, increase the ohmic and conductor losses

thus decreasing the antenna gain. In order to include these losses in the simulation, the

metal thickness has been included in the simulation, and as a result the radiation

efficiency dropped to 8%.

3.4.2   The Second Design

In order to improve the radiation efficiency the ground plane was removed from

beneath the antenna. This removal caused the resonant frequency to shift up to 4 GHz,

therefore the antenna size was increased to shift the frequency back to 2.4 GHz. The

simulated radiation efficiency increased up to 55%.

The antenna geometry after removing the ground plane from beneath the antenna

is as shown in Figure 3.8. The antenna width was increased by a factor of 2 related to the

initial design.
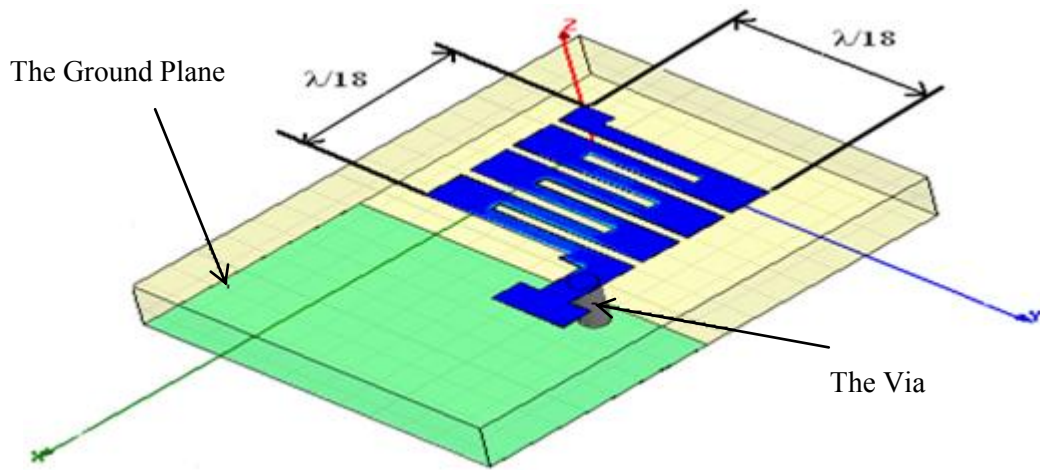
Figure 3.8: The Antenna Geometry for the Second Design

Figure 3.9 illustrates the simulated return loss. As seen the bandwidth also increased by a factor of two relative to the initial design.
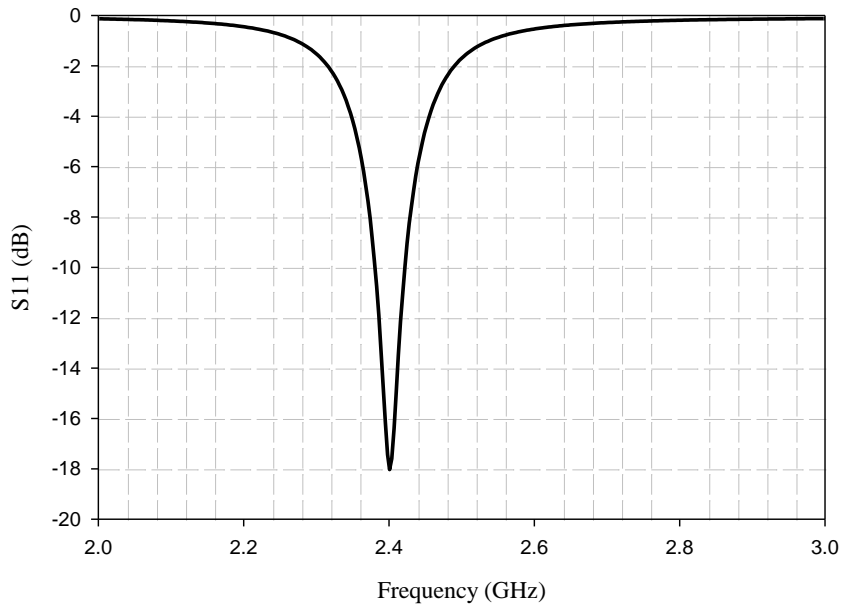


Figure 3.9: The Simulated Return Loss for the Second Design

Figure 3.10 shows the simulated 3D radiation pattern. The radiation pattern became perfectly omni-directional in the broadside direction, which is similar to dipole antennas. Table 3.2 summarizes the simulated characteristics of the second antenna design.

38
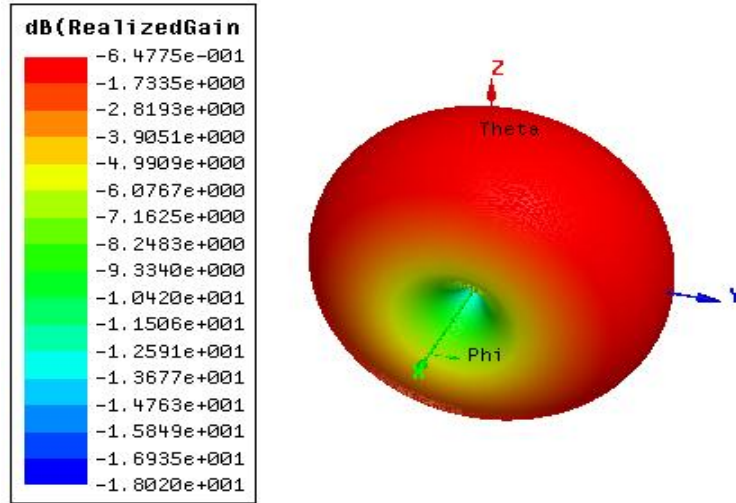
Figure 3.10: The Simulated 3D Pattern for the Second Design

Table.3.2: Antenna Parameters for the Second Design

| Maximum Return loss | 17 dB |
|---|---|
| Directivity | 1.56 |
| Peak gain | 0.86 |
| Radiation Efficiency | 55% |
| ka | 0.24 |
| 10 dB Return Loss BW | 1% |

As noticed when the ground plane has been removed the simulated efficiency increased by a factor of 3.6, and the radiation pattern became more omni-directional. This improvement happened because removing the ground plane from beneath the antenna reduces the surface wave loss; these surface waves are excited on microstrip antennas whenever the substrate $\varepsilon_r > 1$ [31]. These waves are incident on the ground plane and follow a zigzag path between the ground plane and the dielectric air interface, until they reach the antenna boundaries and cause radiation [31]. In addition, removing the ground plane makes the electric field waves propagation and launching into the space easier.

Attaching a coaxial connector to the antenna, in the simulation, caused a shift in the resonant frequency, and this shift was dependent on the coaxial connector length. Taking the connector far from the antenna by increasing the 50 ohm feed line length and the ground plane beneath it, reduced the amount of shift (this shift was around 0.5 GHz), but did not eliminate it completely.

This observation was reasonable because the antenna is very small and the coaxial connector, which was bigger than the antenna and very close to the antenna, was adding a coupling capacitance. The capacitances lead to a down-ward frequency shift.

The current distribution was closely examined on the antenna structure. It was observed that there is a high current distribution on the outer conductor of the coaxial connector, which means that there is a radiation from the cable. It was concluded that the simulated efficiency increased in part due to the connector.

The antenna was fabricated to see how the measurement will be affected with the current distribution on the outer conductor of the cable. It was well observed that moving the hand along the coaxial cable was modifying the measured reflection coefficient and the resonant frequency, but in general the resonant frequency was around 2.4 GHz.

This current running over the coaxial feed line can be expected, since there is no ground plane or other conductor to balance the current on the antenna. Furthermore, the via is disturbing the current distribution on the ground plane. Simply put, the antenna is like a monopole without a ground plane. Finding the correct feeding type is not easy, since one of the common and important characteristics about small antennas is that their

correct feeding is rarely perfectly balanced, as with a dipole, or significantly unbalanced, as with a microstrip patch [18].

A rectangular patch antenna was designed and fabricated in order to compare the resonant frequency sensitivity to the coaxial cable. It was found that even the patch antenna is sensitive to the cable length, but it is the return loss peak not the resonant frequency or $S_{11}$ phase that is sensitive. It was observed that there is not current on the outer conductor of the connector with the conventional patch antenna in both the measurement and the HFSS simulation.

### 3.4.3  The Final Design

In the second design there was radiation from the coaxial connector. In order to solve this problem and be able to measure the antenna characteristics correctly, the ground plane width was increased until the antenna has been balanced. Figure 3.11 illustrates the final design geometry.

The ground plane dimension has been determined experimentally by measuring the input impedance using a vector network analyzer (VNA) for different ground plane sizes, after which copper tape has been added until the resonant frequency stabilizes, like the conventional patch antenna. In general, this antenna needs this ground plane width to remove the unbalanced current effect by absorbing the charge flow, therefore, minimizing the current flow on the outer conductor of the coaxial connector. It was observed that the width of the ground plane seems to be more sensitive than the length, and this can be attributed to the fact that the induced currents are mainly concentrated along the width of the ground plane and near to the antenna element [38]. Its shape does

not measurably affect the antenna performance, and therefore, it can be bent to minimize the total size with minimal impact.
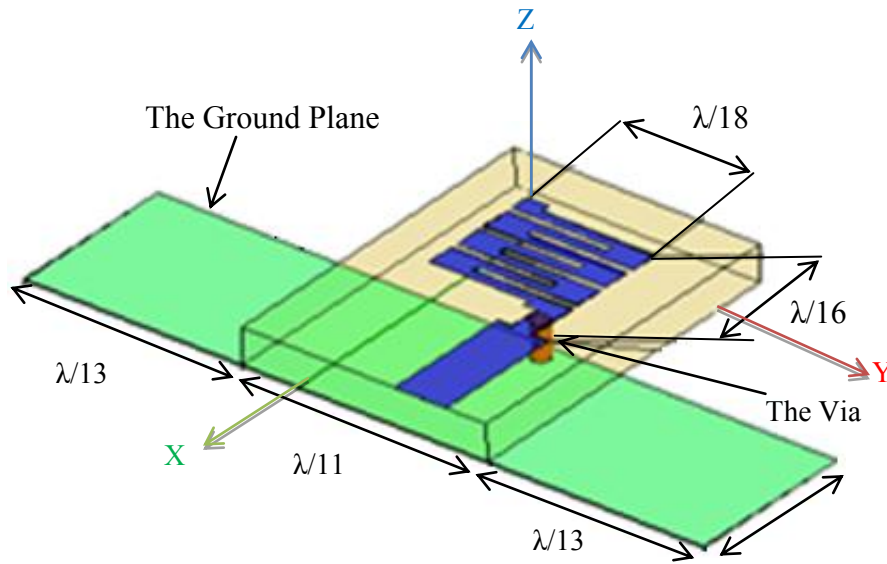


Figure 3.11: The Final Design Geometry

The antenna dimensions are illustrated in Figure 3.12 and Table 3.3. As seen the antenna size was changed after increasing the ground plane size, since increasing the ground plane size shifted the frequency down to some extent.
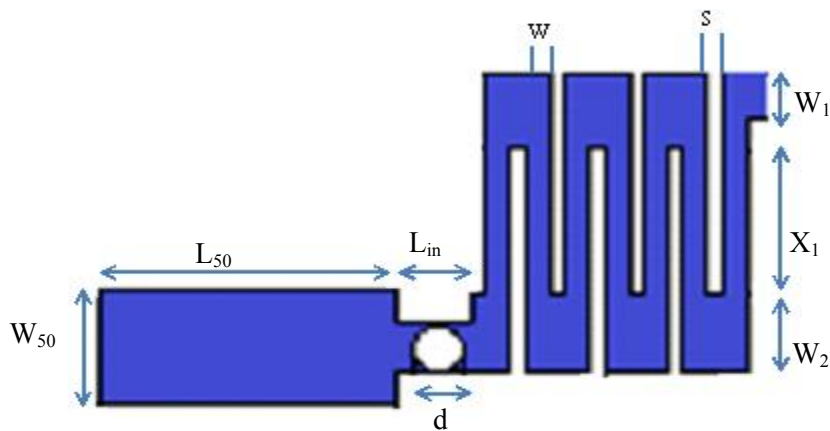


Figure 3.12: The Final Antenna Design Dimensions

Table.3.3: The Final Antenna Design Dimensions in mm

| $L_1$ | 0.5 | $L_{50}$ | 6 |
|---|---|---|---|
| $W_1$ | 1 | S | 0.3 |
| $W_2$ | 1.6 | W | 0.5 |
| $X_1$ | 3 | $L_{in}$ | 1.5 |
| $W_{50}$ | 2.36 | d | 0.8 |

The measured and simulated return losses are illustrated in Figure 3.13. As seen the simulated data fit the measured data, except that the 10 dB return loss bandwidth was increased by 0.65%. This increase could be attributed to the thickness of the added copper tape to the ground plane, which was not accounted for in the HFSS simulation.
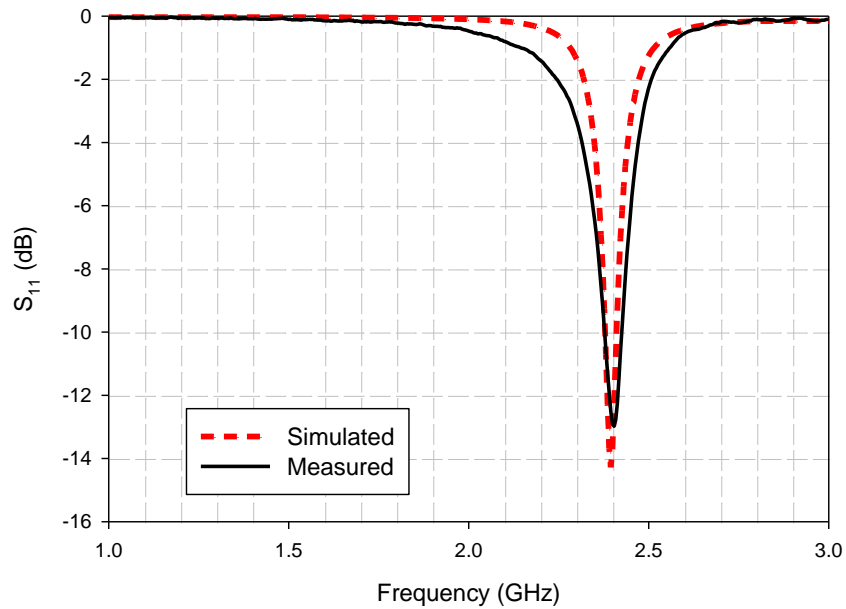


Figure 3.13: The Measured vs. Simulated Return Loss of the Final Design

The simulated 3D pattern is illustrated in Figure 3.14, as seen increasing the ground plane did not affect the radiation pattern, relative to the second design.
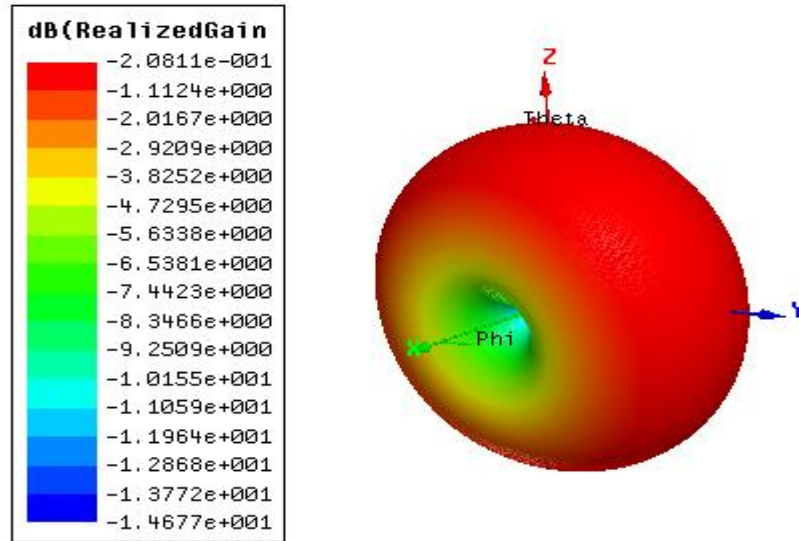
Figure 3.14: The Simulated 3D Pattern of the Final Design

Figure 3.15 shows the measured E- and H-plane radiation patterns. The measurements were performed inside an anechoic chamber using a commercially available antenna as the transmitting antenna and the designed antenna as the receiving antenna. The antennas were separated in accordance to apply testing in the far field region. The H-plane test consisted of rotating the antenna along the azimuth axis from $0^o$ to $360^o$ with an elevation angle of $0^o$ (YZ-Plane), according to Figure 3.11. The orientation of the transmitting antenna for this pattern was set to be vertical to the receiving antenna. For the E-plane measurement, the receiving antenna is rotated $90^o$ perpendicular to the H-plane, after which, the azimuth rotation from $0^o$ to $360^o$ is executed along the E-plane (XY-Plane).
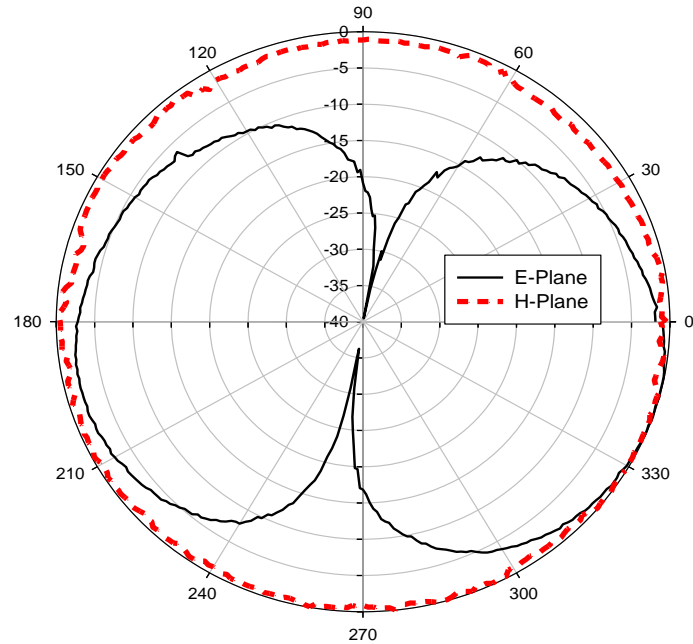
Figure 3.15: The Measured Radiation Patterns of the Final Design

### 3.4.4  Efficiency and Gain Measurements

In order to determine the efficiency of the final antenna design, a cubical configuration of copper measuring $(\lambda/3)^3$ was used as the Wheeler Cap, Figure 3.16. The size of the Wheeler Cap was selected to push the interior modes to higher frequencies resulting in a much sparser mode spectrum [25].



Figure 3.16: The Cubical Wheeler Cap

The efficiency has been determined by measuring the reflection coefficients using a VNA, and then the data has been processed to find the input resistance with and without the cap in order to determine the radiation resistance and the loss resistance. It was observed that the antenna behaves more like a series RLC near its resonant frequency, therefore, eq.2.18 was used to calculate the efficiency.

The gain has been measured using the 3-antenna method using two commercial antennas of gain 9 and 12 dBi in an anechoic chamber by following the same procedures for measuring the E-plane radiation pattern in the previous sub-section of this chapter. Figure 3.17 shows the measured maximum gain over the frequency.
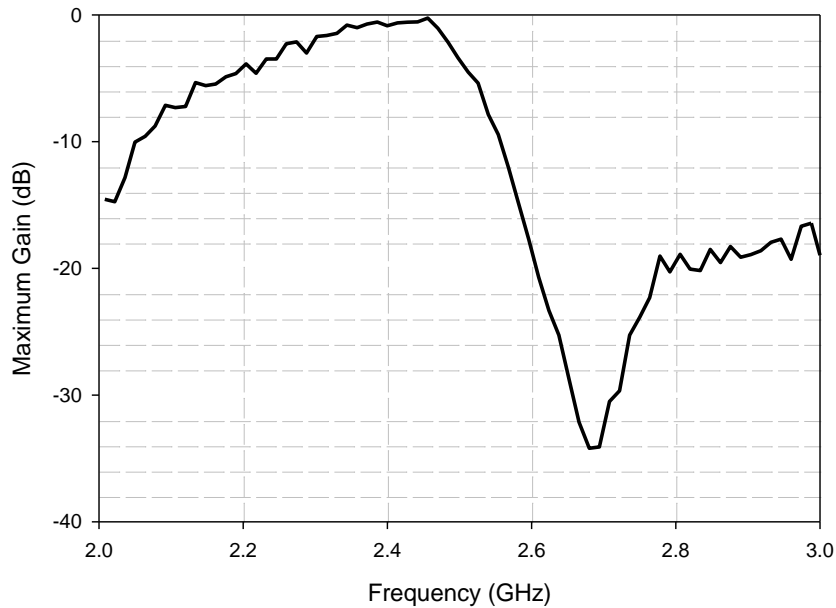


Figure 3.17: The Measured Maximum Gain of the Final Design

The formula that has been used for measuring the gain is as expressed below:

$$G_{antenna} = S_{21}^{antenna,ref1} + S_{21}^{antenna,ref2} - S_{21}^{ref2,ref1} - P_l, \quad (3.3)$$

$$P_l = 10 \log \left( \frac{\lambda}{4\pi d} \right)^2 , \qquad\qquad\qquad (3.4)$$

Where $P_l$ is the path loss, d is the distance between the two antennas which should be fixed during the three measurements, $S_{21}^{antenna,ref1}$ is the measured $S_{21}$ between the designed antenna and the reference antenna of gain 12 dBi, $S_{21}^{antenna,ref2}$ is the measured $S_{21}$ between the designed antenna and the reference antenna of gain 9 dBi, and $S_{21}^{ref1,ref2}$ is the measured $S_{21}$ between the two reference antennas—this formula is based on the Friis transmission equation [7].

The efficiency was also calculated using the gain/directivity method. Based on the measured gain using the 3-antenna method and the simulated directivity using Ansoft HFSS 11, eq.2.17 was applied.

Table 3.4 lists the measured antenna characteristics at the operating frequency. As seen, both methods for measuring the efficiency give similar results. It was found that the Wheeler Cap method is easier to implement, but with unrepeatable results as the variability was around 5%. The gain/directivity method was repeatable with uncertainty of approximately 6%. The uncertainty in the gain/directivity method can be explained by cable effects and VNA calibration errors.

Table.3.4: The Measured Antenna Parameters for the Final Design

| | |
|---|---|
| Maximum Return loss | 14.2 dB |
| Simulated Directivity | 1.64 |
| Peak gain | -0.86 dB |
| Radiation Efficiency using the Wheeler Cap Method | 44% |
| Radiation Efficiency using the Gain/Directivity Method | 49.7% |
| ka | 0.26 |
| 10 dB Return Loss BW | 2% |

In Table 3.4, *ka* represent the antenna size excluding the ground plane and the feed line, as there is no critical radiation from these parts and experimental testing verified that the antenna performance was unaffected by a reduction in the ground plane length by up to ~50% of the dimension shown in Figure 3.11. As aforementioned, the ground plane can be bent to minimize the total size without affecting the antenna performance.

3.5 Conclusion

Different miniaturization techniques, challenges, and their effect on the radiation characteristics have been presented. It was found that the miniaturization process affects directly the gain, bandwidth, and efficiency—it can also affect the antenna polarization, however, it was shown that the reduction of size did not result in a significant reduction of the radiation characteristics in the presented antenna design.

A low cost, easy to fabricate, planar meandered line antenna operating at 2.4 GHz was designed, fabricated, and measured. Good agreement occurred when comparing the expected and measured response for this electrically small antenna. It was found that this antenna works well at the frequency of operation, with good radiation characteristics according to its small electrical size, such as high gain and efficiency, and omni-directional patterns. Therefore, the proposed design should work well in low-power narrow-band sensing applications where a small circuit footprint is desired.

The study of the ground plane effect strengthens the assertion that the ground plane is an important part in antenna design; therefore, the antenna design should not be as a separate component that could be selected in a late design phase of the transceiver layout [38]. Moreover, it was found that feeding a small antenna efficiently is not easy, since the correct feeding of a very small antenna is rarely perfectly balanced or significantly unbalanced.

The gain measurement method that has been used, essentially requiring only an anechoic chamber, is simple in principle but is found to suffer from lack of accuracy. The Wheeler Cap method is the easiest to implement, but has some repeatability challenges.

# CHAPTER 4

# 3D DIPOLE ANTENNA DESIGN

4.1 Introduction

As discussed in chapter two, 3D antennas are preferred for applications that require efficiency concurrently with small size, since these antennas have more efficient use of the available volume by realizing relatively long antenna lengths. 3D antennas are also beneficial in opening up internal volume for other uses, such as storage room for batteries or other circuit elements.

Dipole antennas are one of the oldest, cheapest, and simplest antennas that offer good performance. They can be easily fabricated in different shapes and configurations. In [39], a dipole antenna has been fabricated on a spherical configuration, which provided very good performance due to utilizing the occupied volume to the greatest extent. In [40], a dipole antenna has been printed on a pyramid configuration. The antenna was fabricated easily on this configuration; however, the pyramid configuration provided low gain although the antenna exhibited large electrical size. The low gain is due to the high percentage of cancelled radiated fields related to the way that the dipole arms were rotated.

This work focuses on the analysis, design, and fabrication of 2.4 GHz 3D dipole antennas on a cube configuration providing simplicity and conformal packaging. The

antenna is fabricated on two sides of the cube and connected to a balanced-to-unbalanced line transition on a third side. The base of the cube serves as a ground plane for the microstrip feed line. It was found that the cube configuration results in a high gain, small antenna. Good agreement between the simulated and measured response was obtained. *Ka* of the final design and its measured gain are 0.55 and 1.69 dBi, respectively.

In this chapter, a background theory about the radiation mechanism of dipoles and the transition between unbalanced to balanced structures using a parallel plate balun are discussed. The study of the cube configuration started by designing a conventional planar half wave dipole antenna, then the same dipole antenna was designed on one face of the cube to test the effect of bending the parallel plate line. Finally, the arms of the dipole have been meandered to minimize the length of the antenna, before the antenna was designed on the cube.

## 4.2 Background Theory

A dipole antenna can be defined as a lossless conductive two wire flared transmission line where the radiating fields do not cancel each other due to the separation of the wires [40]. Usually the two conductive wires are fed at the center [41]. The dipole length determines possible current distributions in modes [41]; classically, a dipole antenna is formed by two quarter wavelength conductors placed back to back for total length of $\lambda/2$.

Dipole antennas are usually viewed as standing wave antennas, as their radiation is the result of a standing wave electric current [41]. Assuming that two identical wires

are running parallel to each other, the current of each wire will be of the same magnitude but have $180^o$ phase difference at any point along the wire, Figure 4.1.



Figure 4.1: Two-Wire Transmission Line

If the spacing between the two wires is much smaller than $\lambda$, the radiated fields from each wire will cancel each other; ideally the net radiated fields will be zero. Once a section of the two wires begins to flare by an angle of $\theta$, Figure 4.2, the radiated fields will not be cancelled completely. When this flared section is rotated $90^o$ forming the commonly used dipole antenna, the radiation will be maximized.
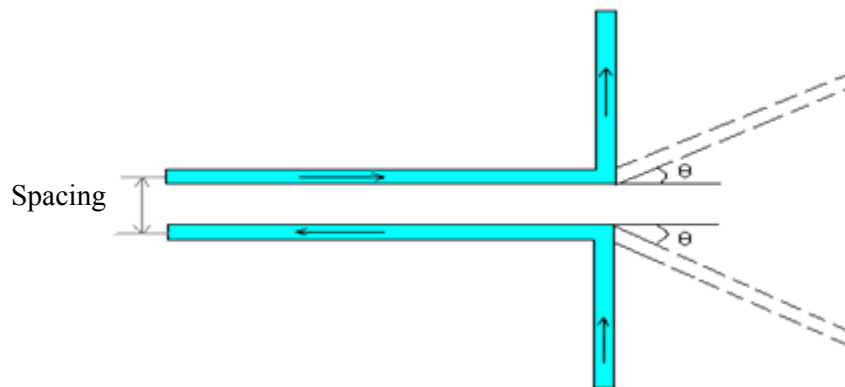


Figure 4.2: Flared Transmission Line and Linear Dipole

Symmetric dipole antennas require a balanced feed as shown in Figure 4.2. Since the connection to the signal source is usually unbalanced, such as a coaxial feed, a balun is needed to transform the unbalanced feed (coax and microstrip line) to a balanced dipole antenna.

In this work, a $\lambda/4$ parallel plate waveguide transmission line is used as a balun, Figure 4.3. A parallel plate waveguide can support TM, TE, and TEM modes [42]. Simply, it consists of two strips of a width much larger than the separation between them in order to ignore the fringing fields [42].
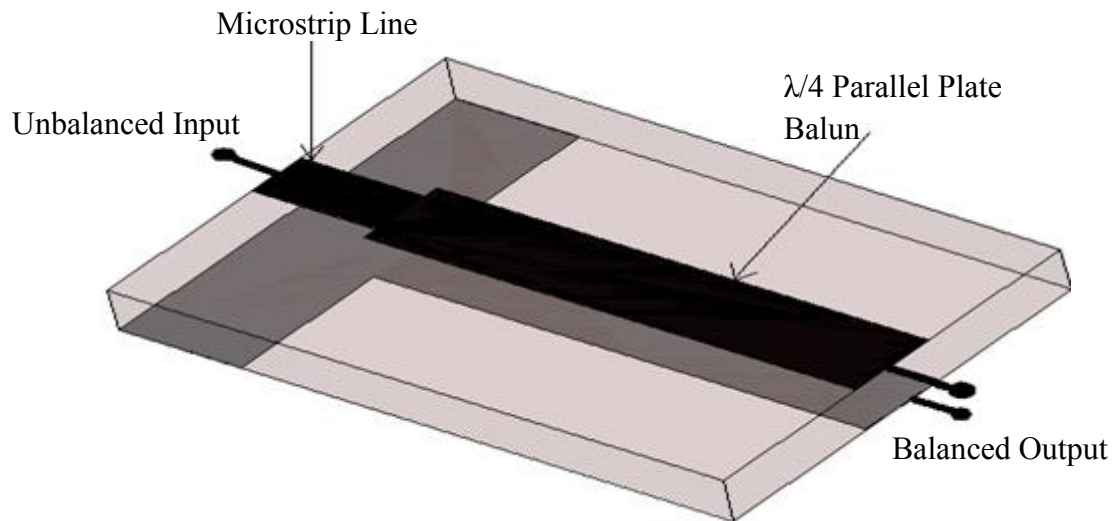


Figure 4.3: Parallel Plate Balun

The two strips need to be $\lambda/4$ in length in order to provide high impedance at the dipole antenna side, cancelling the unbalanced current coming from the ground of the unbalanced microstrip feed line [40]. This is the approach used with the Bazooka balun [41].

4.3 Conventional Planar Dipole Antenna Design (First Iteration)

In this section, a conventional planar half wave dipole antenna operating at 2.4 GHz is designed, fabricated and measured. The substrate is Rogers/RT Duroid 6010 with a nominal dielectric constant ($\varepsilon_r$) of 10.2, and thickness of 50 mils. The optimization

process includes the design of a balanced radiator (regular dipole) and an optimized balun for this balanced radiator.

The proposed antenna geometry is shown in Figure 4.4, where the flat dipole is formed by two symmetric rectangular strips of dimensions $L_a$ =23 mm long and $W_a$ = 1 mm wide. These arms are fabricated on both sides of the substrate. The dipole is center-fed by a $\lambda_g/4$ parallel plate balun, followed by a matching line and a $\lambda_g/10$ 50 ohm microstrip line.

The values for the design parameters were selected from a parametric study that has been carried out to achieve the optimum performance and are indicated in Table 4.1 and Figure 4.5. The resonance frequency of the antenna is determined by the overall length of the dipole arms. The dielectric substrate covers only a finite region around the dipole and a low percentage of the radiated fields; therefore, the resonant length is not directly proportional to the inverse of the square root of $\varepsilon_r$ [43]. It was found that the effective dielectric constant is approximately 2 and the resonant dipole's length is 0.36 $\lambda_o$, for the reason explained above. The length of the parallel plate balun was also optimized separately for best performance.

The matching line length, matching line width, parallel plate balun width, microstrip line ground width, and arm width were all optimized to match the antenna input impedance to 50 ohms. Moreover, the shape of the arm was tapered in its center to improve the matching. It was found that the width of the parallel plate balun and width of the arms slightly affect the resonant frequency. The impedance of the parallel plate

transformer is approximately 64 ohms and the estimated impedance of the matching line

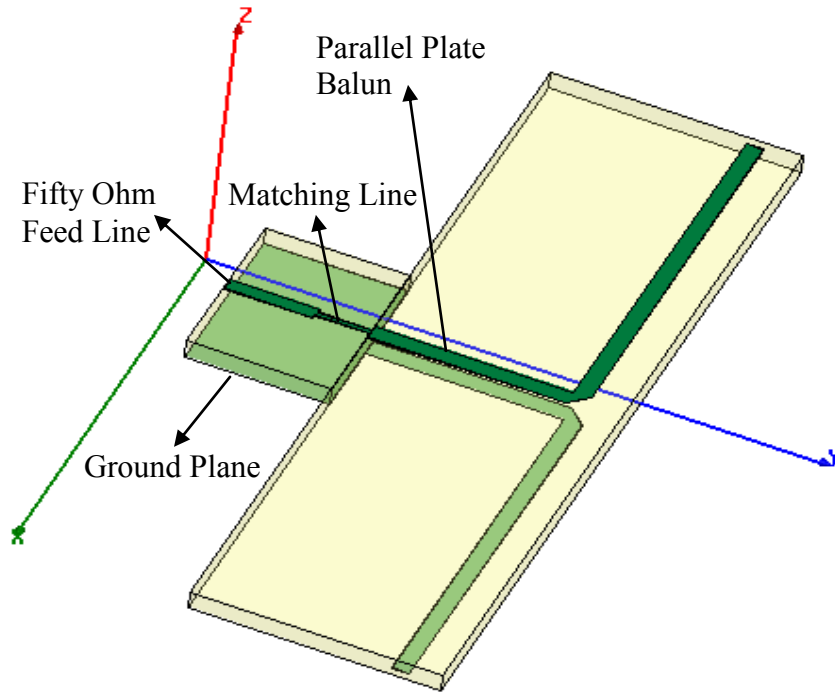is 71ohms with an electrical length of $\lambda_g/17$.



Figure 4.4: The Geometry of the Conventional Planar Dipole Antenna Design
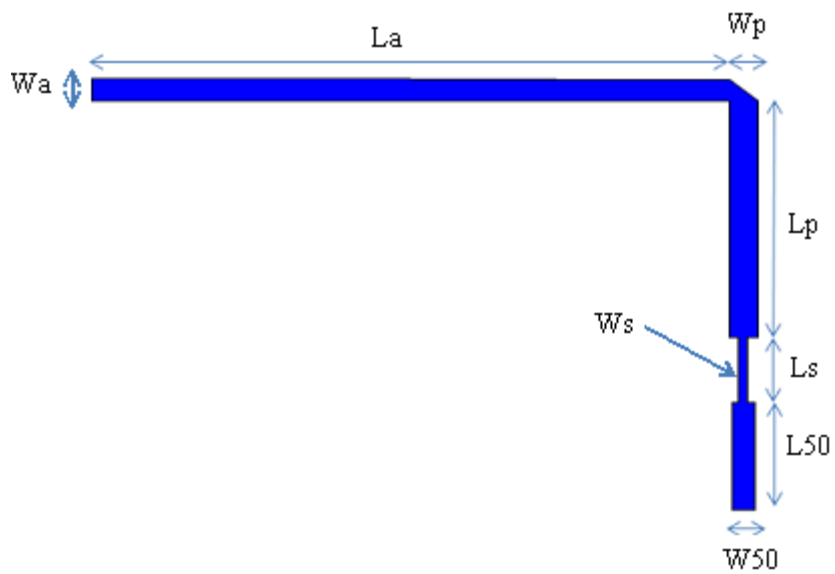


Figure 4.5: The Conventional Planar Dipole Antenna Design Dimensions

Table.4.1: The Conventional Planar Dipole Antenna Design Dimensions in mm

| $L_a$ | 23 | $L_s$ | 3 |
|---|---|---|---|
| $W_a$ | 1 | $W_s$ | 0.3 |
| $L_p$ | 11 | $L_{50}$ | 5 |
| $W_p$ | 1 | $W_{50}$ | 0.8 |
| Ground Plane Width | 10 | Ground Plane Length | 8 |

The measured and simulated return loss is shown in Figure 4.6. As seen from the figure, the simulated data matches well the measured performance. The simulated data was obtained assuming a 100 mm-long coaxial feed cable.



Figure 4.6: The Measured vs. Simulated Return Loss of the Conventional Planar Dipole Antenna Design

Figure 4.7 shows a comparison between the measured and simulated return loss using 9 mm-long and 100 mm-long coaxial feed cables. The 100 mm-long cable gives a better prediction of the measured data, and as discussed in section 2.4 the coaxial feed

effect cannot be ignored in the measurements. Therefore, all the simulated results that follow in this chapter were obtained assuming a 100 mm-long coaxial feed cable.
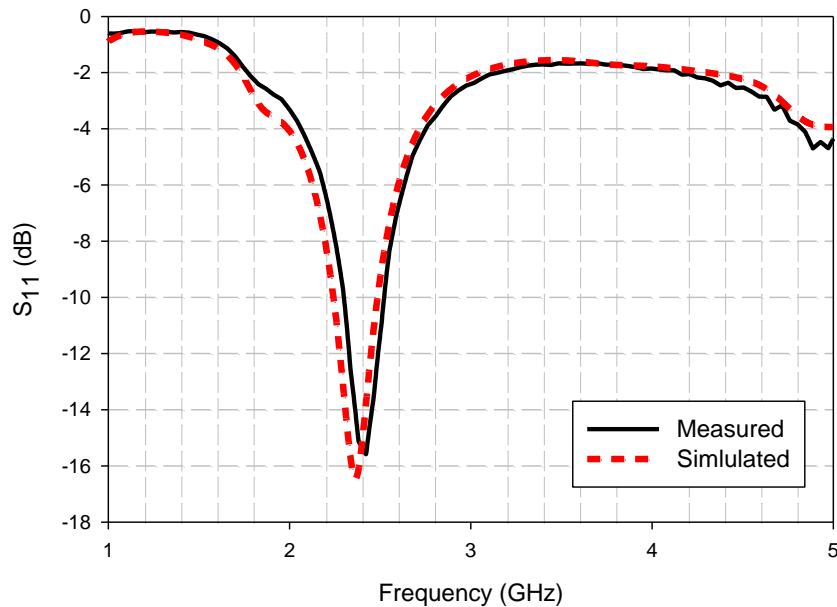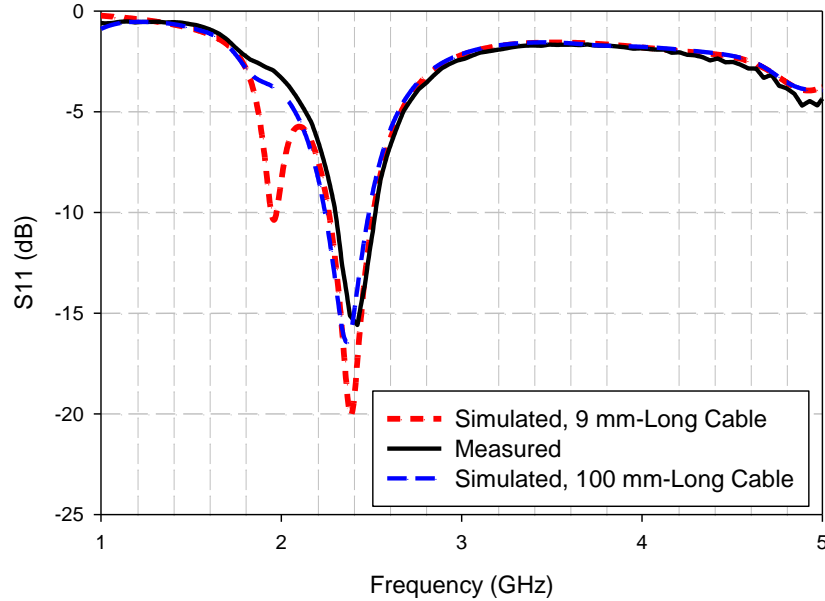


Figure 4.7: The Measured vs. Simulated Return Loss of the Conventional Planar Dipole Antenna Design Using 9 and 100 mm-Long Cable

It is noticed in Figure 4.7 that there is a strong resonance at 1.9 GHz for the simulation that uses a 9 mm-long coaxial feed cable. The measurements proved that the antenna is unbalanced at this frequency as the resonant frequency and the peak return loss were affected by movement in the coaxial feed cable. An HFSS simulation using a 100 mm-long cable also predicted that the antenna is unbalanced at this frequency, as there is an 8 dB difference in the return loss compared to the simulation that uses a 9 mm-long cable. The reason why the antenna is unbalanced at this frequency could be that it is not a half-wave dipole at this resonance.

The simulated 3D pattern is shown in Figure 4.8. A perfect omni-directional pattern in the broadside direction was obtained as expected for a half wave dipole

antenna. Figure 4.9 shows the measured co- and cross-polarized radiation patterns in the E- and H-planes. The measurements were performed inside an anechoic chamber following the same procedures used in section 3.4.3. The E-plane test was carried out by rotating the antenna along the azimuth axis from $0^o$ to $360^o$ at an elevation angle of $0^o$ (XZ-Plane), relative to the coordinate system in Figure 4.4. For the H-plane the receiving antenna was rotated $90^o$ perpendicular to the E-plane, after which, the azimuth rotation from $0^o$ to $360^o$ was executed along the H-plane (YZ-Plane).
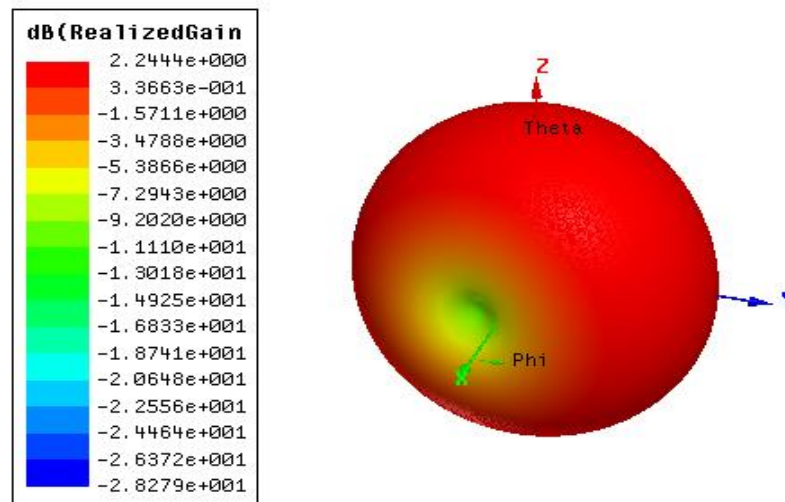


Figure 4.8: The Simulated 3D Pattern for the Conventional Planar Dipole Antenna Design
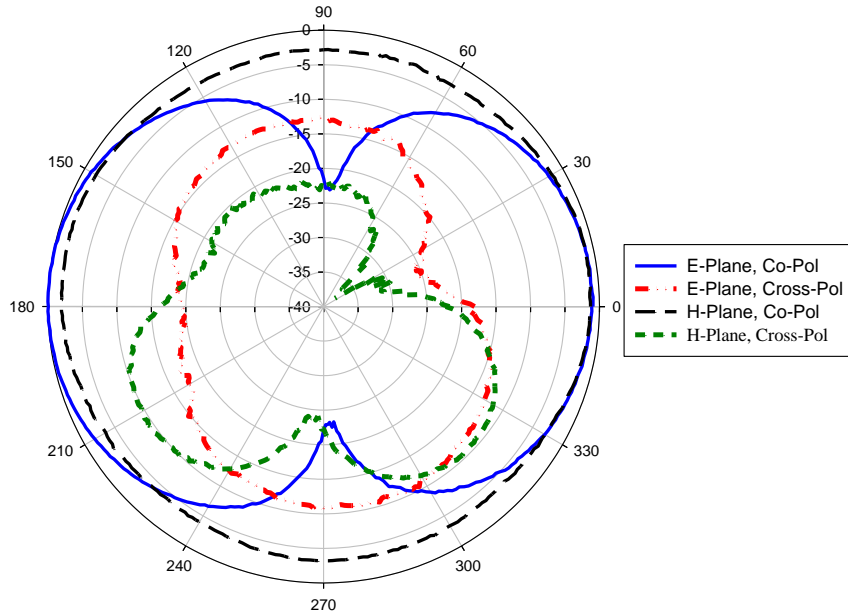
Figure 4.9: The Measured Radiation Patterns for the Conventional Planar Dipole Antenna Design

The gain has been measured using the 3-antenna method using the same two commercial antennas that were used in section 3.4.4. The measurement was performed by following the same procedures above for measuring the co polarized E-plane radiation pattern. Figure 4.10 shows the measured maximum gain over frequency.
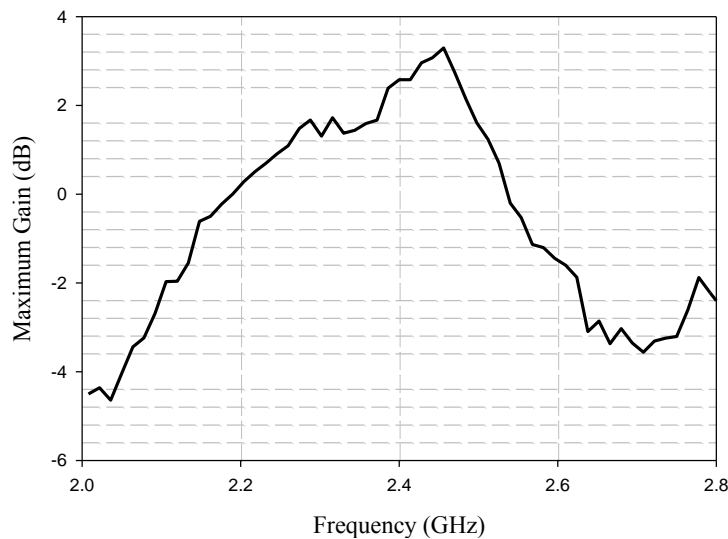


Figure 4.10: The Measured Maximum Gain for the Conventional Planar Dipole Antenna Design

Table 4.2 shows a comparison between the simulated and measured antenna parameters at the operating frequency. The measured results agree fairly well with the simulated results.

Table.4.2: Comparison between Simulated and Measured Antenna Parameters for the Conventional Planar Dipole Design

| Parameter | Measured | Simulated |
|---|---|---|
| Directivity | ---------- | 1.75 |
| 10 dB Return Loss BW | 9.3% | 10.3% |
| Maximum Return Loss (dB) | -15.5 | -16.4 |
| Peak Gain (dBi) | 2.57 | 2.24 |
| ka | 1.15 | -------- |

4.4 Dipole Antenna on One Side of a Cube (Second Iteration)

In order to minimize the occupied volume of the conventional planar dipole antenna and to test the effect of bending the parallel plate line, the second iteration was designed, fabricated, and measured at the same operating frequency as the conventional antenna. The substrate material was not changed. The antenna geometry is shown in Figure 4.11. Table 4.3 illustrates the antenna dimensions, which are the same as those for the first iteration design.
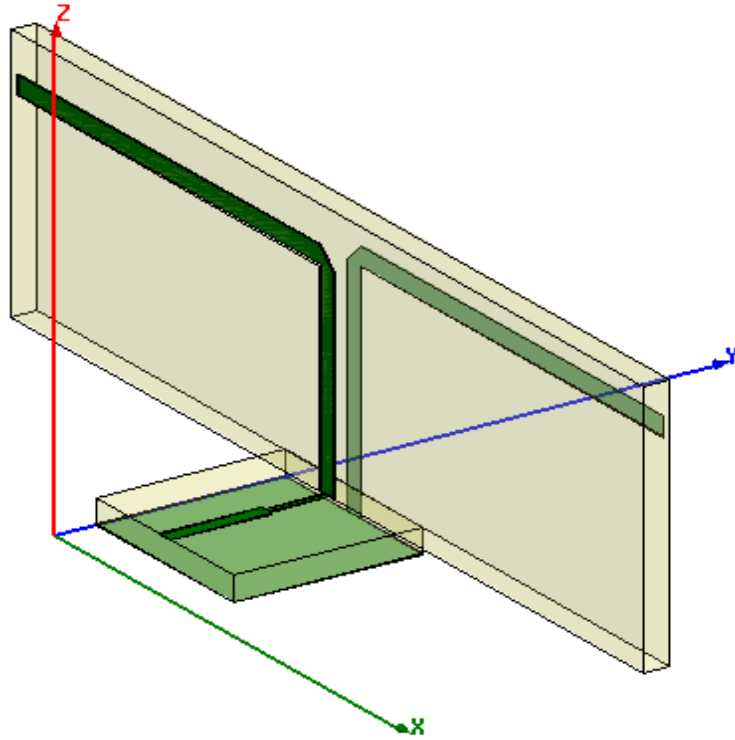
Figure 4.11: The Geometry of the Second Dipole Antenna Iteration

Table.4.3: The Second Dipole Iteration Dimensions in mm

| $L_a$ | 23 | $L_s$ | 3 |
|---|---|---|---|
| $W_a$ | 1 | $W_s$ | 0.3 |
| $L_p$ | 11 | $L_{50}$ | 5 |
| $W_p$ | 1 | $W_{50}$ | 0.8 |
| Ground Length | 9.27 | Ground Width | 10 |

The measured vs. simulated return loss for the second iteration is illustrated in Figure 4.12. The results show that bending the parallel plate balun does not have a critical effect on the resonant frequency and input impedance.
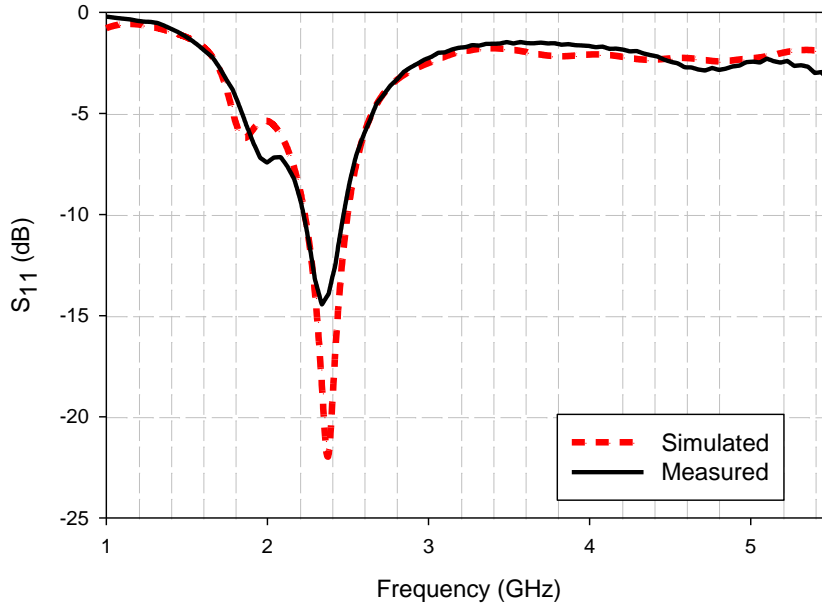
Figure 4.12: The Measured vs. Simulated Return Loss of the Second Dipole Iteration

The simulated 3D pattern is illustrated in Figure 4.13. The plot shows that the simulated 3D pattern and peak gain have not changed with bending the parallel plate balun. Figure 4.14 shows the measured radiation patterns. The measurements were performed by following the same procedures outlined in section 4.3.



Fig.4.13: The Simulated 3D Pattern for the Second Dipole Iteration
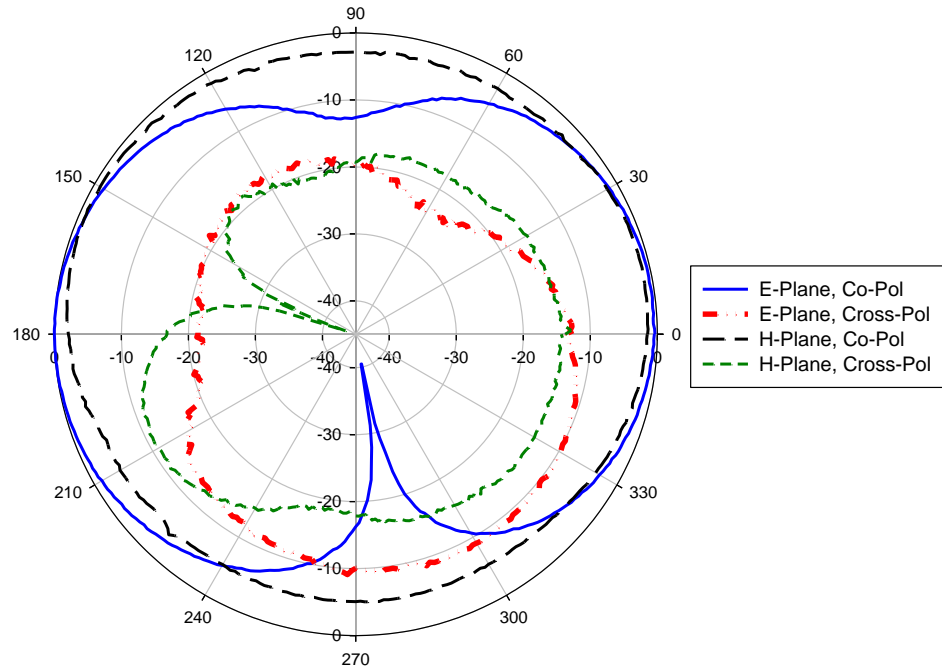
Figure 4.14: The Measured Radiation Patterns for the Second Iteration

Figure 4.15 shows the measured maximum gain for the second iteration. The measurement was carried out following the same procedures used for measuring the maximum gain along the co polarized E-plane in section 4.3.
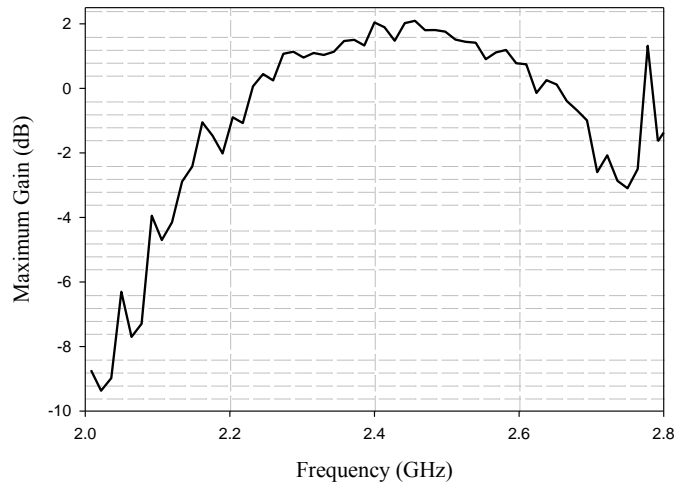


Figure 4.15: The Measured Maximum Gain for the Second Iteration Design

Table 4.4 shows a comparison between the measured and simulated antenna parameters at the operating frequency. Good agreement is observed for the simulated and measured results. Consequently, it can be concluded that bending the parallel plate balun does not have a measurable effect on the antenna performance.

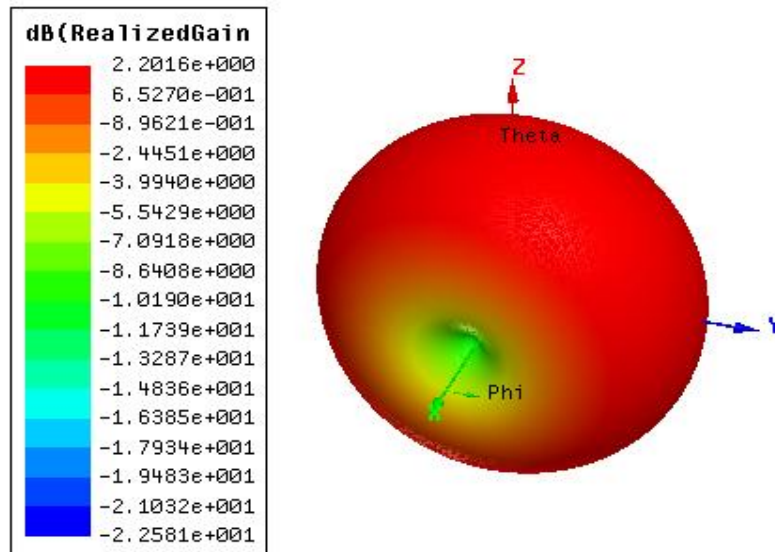Table 4.4: Comparison between the Simulated and Measured Antenna Parameters for the Second Iteration

| Parameter | Measured | Simulated |
|---|---|---|
| Directivity | ---------- | 1.56 |
| 10 dB Return Loss BW | 10.4% | 11.3% |
| Maximum Return Loss (dB) | -14.4 | -21.9 |
| Peak Gain (dBi) | 2.04 | 2.2 |
| ka | 1.15 | -------- |

4.5 Meandered Dipole Antenna Design on One Face of a Cube (Third Iteration)

In this section the meandered line approach was employed to minimize the length of the antenna arms. The substrate material that was selected is also the same one used for the first iteration. The antenna geometry is shown in Figure 4.16.
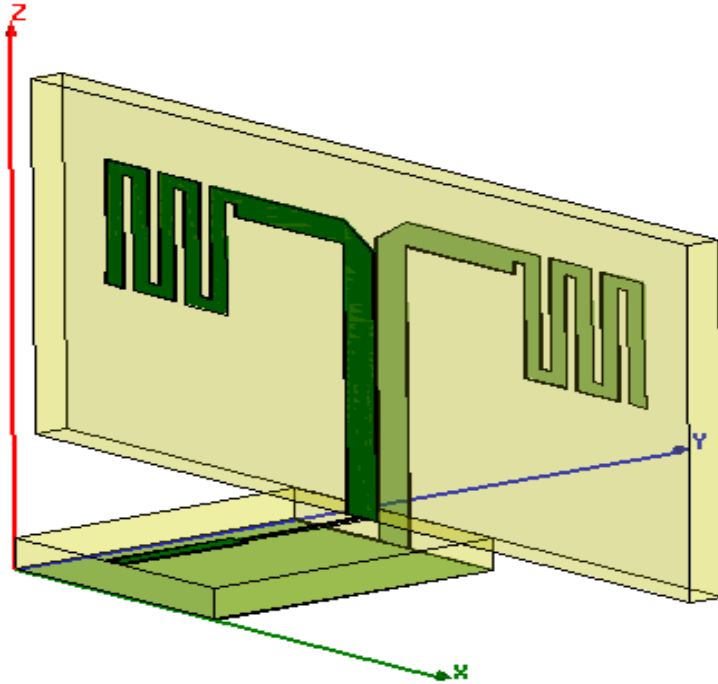
Figure 4.16: The Geometry of the Meandered Dipole Antenna Design

In order to minimize the arm length and keep the resonant frequency at 2.4 GHz, Ansoft HFSS 11 was used to optimize the total length of the meander line of the arms, slot size between sections, and number of meandered sections; (Figure 4.17). To match the input impedance to 50 ohms, the width of the meander line, the width of the parallel plate transformer, and the width and length of the matching line were all optimized. The impedance of the $\lambda_g/4$ parallel plate transformer is 48 ohms and the estimated impedance of the $\lambda_g/10$ matching line is 70 ohms. Table 4.5 shows the meandered dipole antenna dimensions.
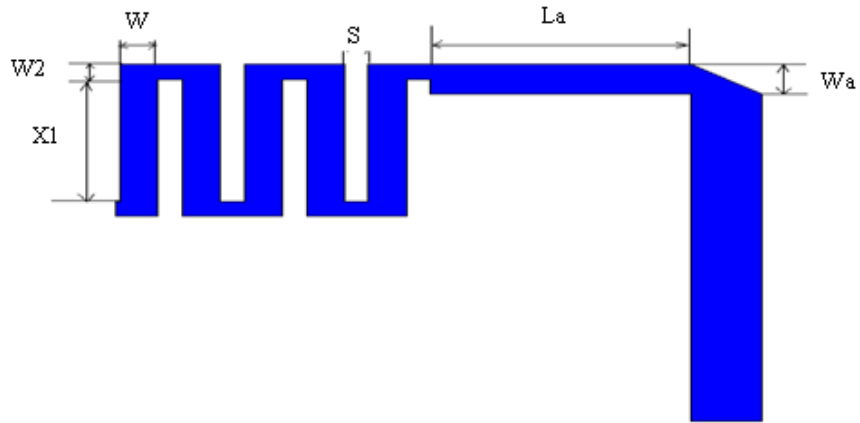
Figure 4.17: The Meandered Dipole Antenna Arms Dimensions

Table.4.5: The Meandered Dipole Antenna Design Dimensions in mm

| $L_a$ | 5.75 | $L_{50}$ | 5 |
|---|---|---|---|
| $W_a$ | 1 | $W_{50}$ | 0.8 |
| $L_p$ | 11 | $X_1$ | 4.1 |
| $W_p$ | 1.5 | W | 0.8 |
| $L_s$ | 5 | $W_2$ | 0.5 |
| $W_s$ | 0.3 | S | 0.5 |
| Ground Length | 11.27 | Ground Width | 10 |

Figure 4.18 shows the measured and simulated return loss of the third iteration. As seen the measured data fit the simulated data, but there was small shift in the frequency, which could be attributed to fabrication errors.
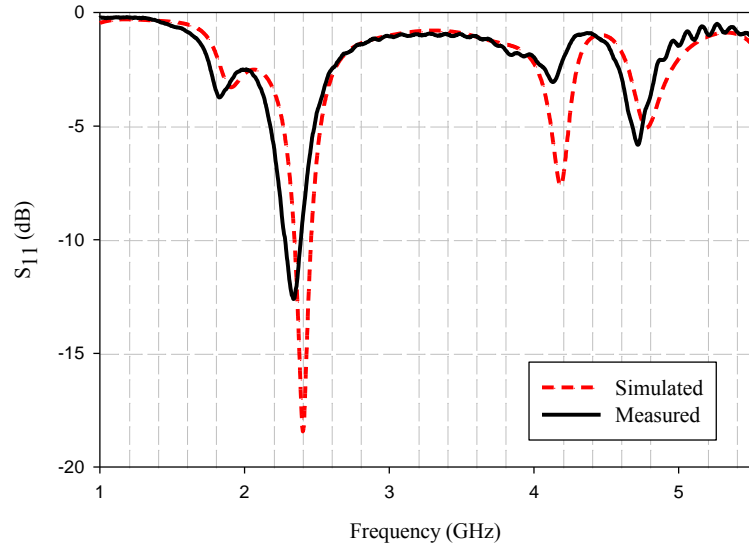
Figure 4.18: The Measured vs. Simulated Return Loss of the Meandered Dipole Antenna Design

The simulated 3D pattern is illustrated in Figure 4.19. As seen, meandering the arms did not affect the gain and the doughnut shape.
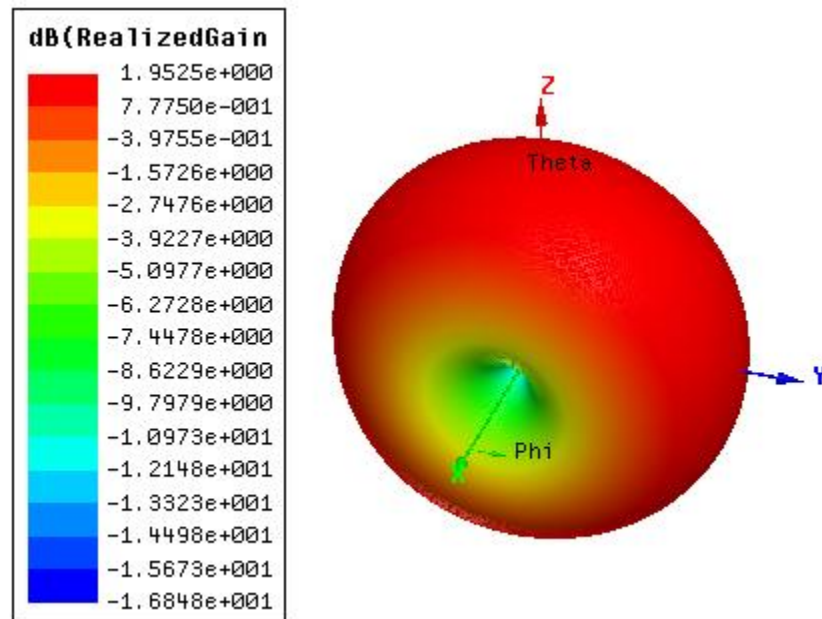


Figure 4.19: The Simulated 3D Pattern for the Meandered Dipole Antenna Design

Figure 4.20 shows the measured E- and H-plane co- and cross-polarized radiation patterns. The measurements were performed using the same procedures followed in section 4.3. The gain has been also measured using the same procedures in section 4.3, Figure 4.21. As seen, the meandered line approach did not affect the antenna polarization.
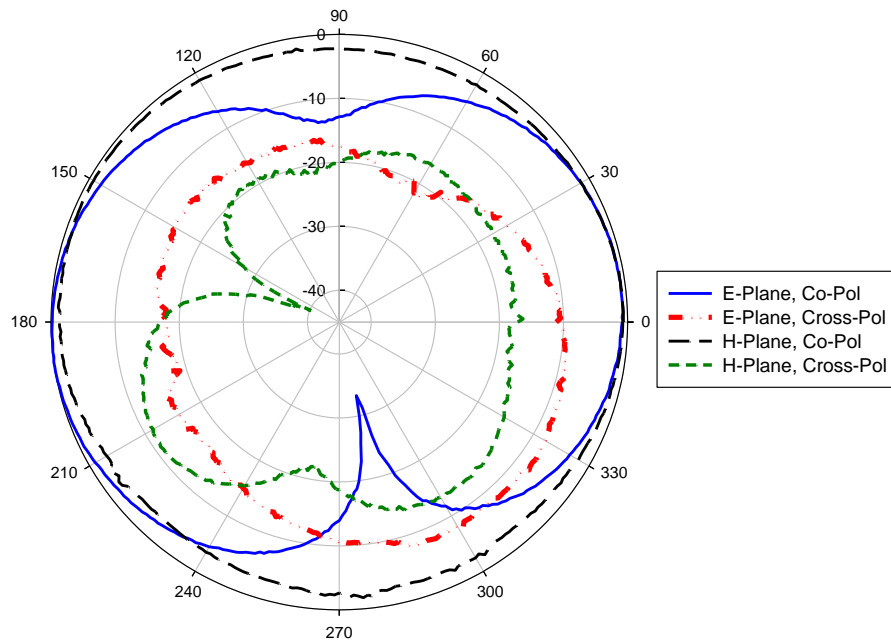


Figure 4.20: The Measured Radiation Patterns for the Meandered Dipole Antenna Design
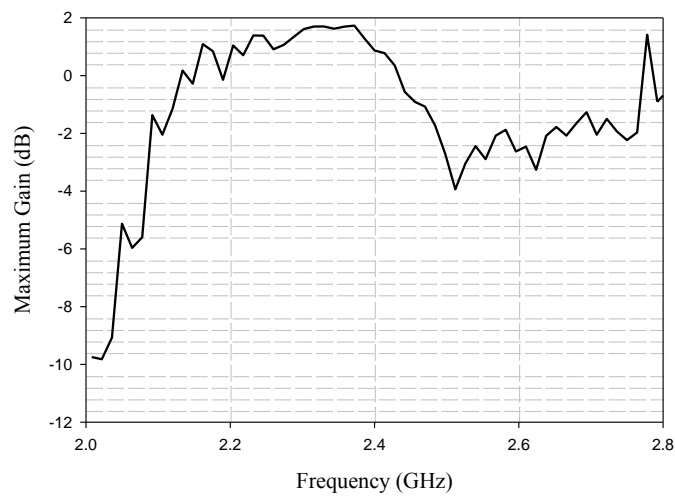


Figure 4.21: The Measured Maximum Gain for the Meandered Dipole Antenna Design

Table 4.6 shows a comparison for the simulated and measured antenna parameters at the operating frequency. There is a good match between the measured and simulated results.

Table.4.6: Comparison between Simulated and Measured Antenna Parameters for the Meandered Dipole Antenna Design

| Parameter | Measured | Simulated |
|---|---|---|
| Directivity | ---------- | 1.6 |
| 10 dB Return Loss BW | 4.7 % | 4.87 % |
| Maximum Return Loss (dB) | -12.4 | -18.6 |
| Peak Gain (dBi) | 1.72 | 1.95 |
| ka | 0.7 | -------- |

It can be concluded from this section that meandering the arm length resulted in minimizing the occupied volume by a factor of 2 with a minimal impact on the gain. However, this approach led to a reduction in the bandwidth by a factor of 2.

4.6 3D Dipole Antenna Design on a Cube (Final Iteration)

After studying the planar dipole antenna design and the radiation mechanism in the first iteration, then studying the bending the parallel plate balun and meandering the arm length, the final iteration was designed as shown in Figure 4.22. The arms were rotated in this way (one goes down and one goes up) to minimize the cancelation of the radiated fields without affecting the balanced current distribution on the dipole arms. The antenna consists of a half wave dipole printed on two sides of the cube connected to the parallel plate balun on the third side. The left hand arm is connected to the microstrip feed line and the right hand arm is connected to the ground plane of the microstrip line.
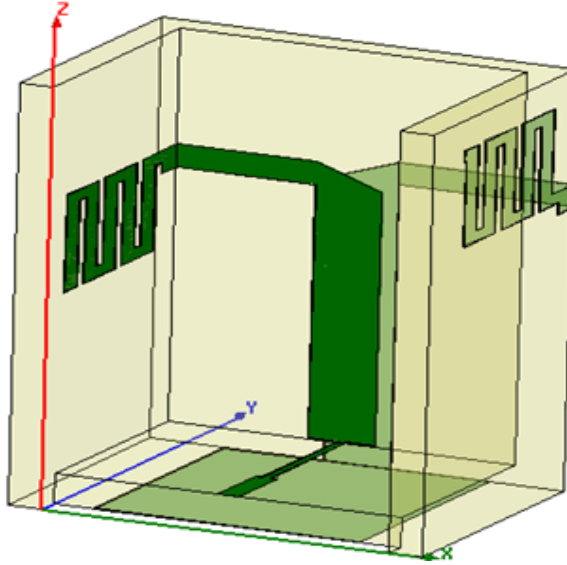
Figure 4.22: The Geometry of the 3D Dipole Antenna Design

The impedance of the $\lambda_g/4$ parallel plate balun is approximately 33 ohms, and the impedance of the $\lambda_g/8$ matching line is 73 ohms. Table 4.7 shows the final iteration dimensions.

Table.4.7: The 3D Dipole Antenna Dimensions in mm

| $L_a$ | 7.78 | $L_{50}$ | 3 |
|---|---|---|---|
| $W_a$ | 1 | $W_{50}$ | 0.8 |
| $L_p$ | 11 | $X_1$ | 3.2 |
| $W_p$ | 2.5 | $W$ | 1 |
| $L_s$ | 6 | $W_2$ | 0.5 |
| $W_s$ | 0.3 | $S$ | 0.5 |
| Ground Length | 10.27 | Ground Width | 10 |

The measured and simulated return loss is illustrated in Figure 4.23. As seen, a good match between the measured and simulated data over a wide frequency range was obtained. The bandwidth was decreased relative to the first iteration by a factor of 5.
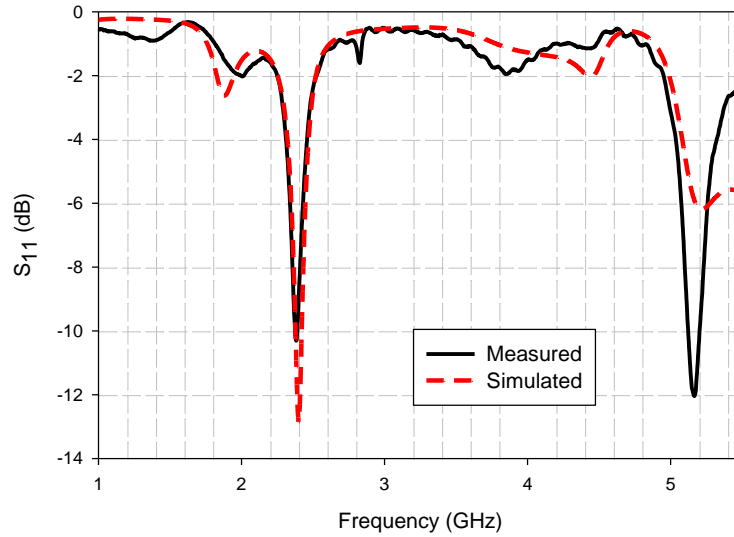
Figure 4.23: The Measured vs. Simulated Return Loss for the 3D Dipole Antenna Design

The simulated 3D pattern is illustrated in Figure 4.24. The doughnut shape is not affected by rotating the arms 90°, and it stayed centered at the same axis. Also, the gain did not deteriorate significantly.
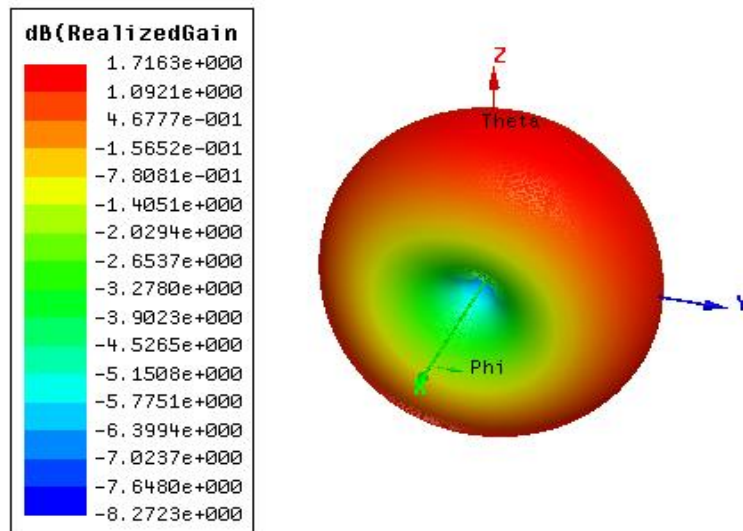


Figure 4.24: The Simulated 3D Pattern for the 3D Dipole Antenna Design

Figure 4.25 illustrates the measured radiation patterns. The measurements were performed by following the same procedures outlined in section 4.3. Rotating the meandered section of the dipole arms 90° relative to the third iteration did not affect the radiation patterns or the polarization, since the antenna polarization remains linear. The gain was also measured and the results are shown in Figure 4.26.

The measured and simulated gain proved that this way of rotating the arms did not result in a high percentage of cancelled radiated fields, as the gain did not decrease significantly. The reason for that is that part of the arms, the meandered section which represent half of the effective length of the arm, was rotated and the rotated sections were placed in an opposite direction relative to each other. Also the radiation pattern measurements proved that rotating the arms in this way did not result in a change of the antenna polarization. This could be related to fact that the current distribution is concentrated on the non-meandered sections of the arms.
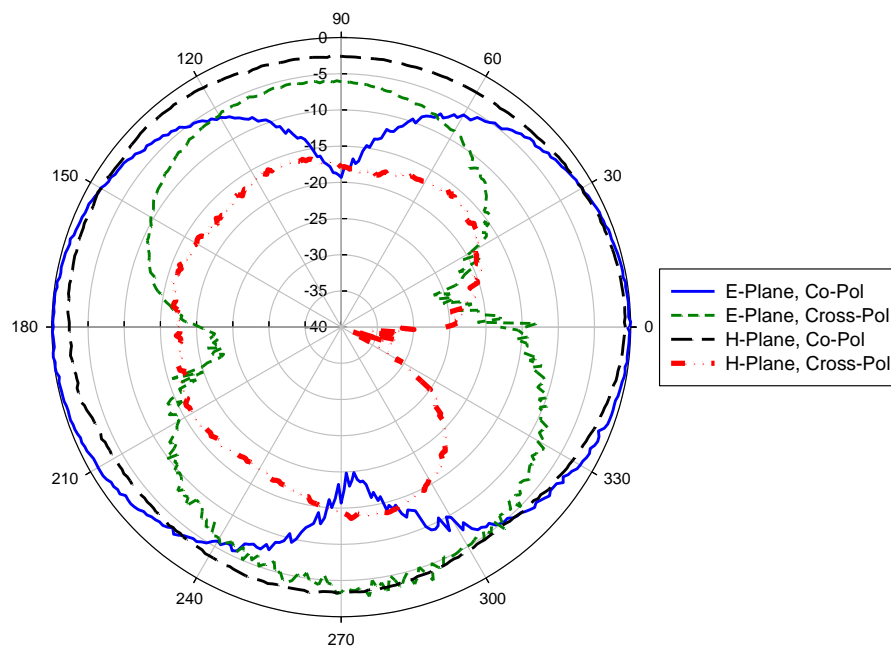
Figure 4.25: The Measured Radiation Patterns for the 3D Dipole Antenna Design
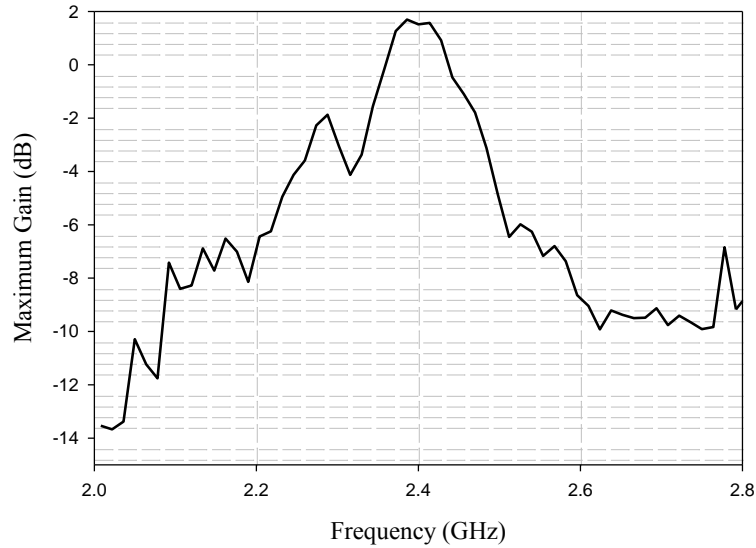
Figure 4.26: The Measured Maximum Gain for the 3D Dipole Antenna Design

Table 4.8 compares the measured and simulated antenna parameters at the operating frequency. Good agreement between the measured and simulated data was obtained.

Table 4.8: Comparison of the Simulated and Measured Antenna Parameters for the 3D Dipole Antenna Design

| Parameter | Measured | Simulated |
|---|---|---|
| Directivity | ---------- | 1.6 |
| 10 dB Return Loss BW | 2 % | 2.24 % |
| Maximum Return Loss (dB) | -10.3 | -12.8 |
| Peak Gain (dBi) | 1.69 | 1.7 |
| ka | 0.55 | -------- |

Table 4.9 compares the measured antenna parameters for all the design iterations. Minimizing the antenna size reduces the gain and return loss bandwidth considerably; however, the final design has high gain for its size, by having an efficient use of the

available volume. The radiation efficiency was measured using the Wheeler Cap method using the same cap used in section 3.4.4. The Wheeler Cap method provided repeatable results but with low accuracy, since there is a small shift in the resonant frequency when the antenna was placed inside the cap to determine the antenna loss resistance.

Table.4.9: Comparison of Measured Antenna Parameters between all the Design Iterations

| Parameter | 1st Iteration | 2nd Iteration | 3rd Iteration | Final Iteration |
|---|---|---|---|---|
| Directivity | 1.75 | 1.56 | 1.6 | 1.6 |
| 10 dB Return Loss BW (%) | 9.3 | 10.4 | 4.7 | 2 |
| Maximum Return Loss (dB) | -15.5 | -14.4 | -12.4 | -10.3 |
| Peak Gain (dBi) | 2.57 | 2.04 | 1.72 | 1.69 |
| Radiation Efficiency Using the Wheeler Cap Method | 89.3% | 83.8% | 67.6% | 64.17% |
| ka | 1.15 | 1.15 | 0.7 | 0.55 |

*. *Ka* represents the overall antenna structure including the feeding network.

For the purpose of comparison between all the design iterations and the other miniaturized small antennas, Figure 4.27 was created. Figure 4.27 shows the gain over quality factor ratio for all the design iterations compared with the optimal gain over quality factor ratio limit. As discussed in section 2.3, small antennas with narrow bandwidths can exceed Harrington's maximum gain limit significantly, therefore, the optimal limit was calculated based on eq.2.12 for the radiation Q limit and a fixed upper gain limit of 3. This ratio was calculated for each of the design iterations based on the measured maximum gain and the measured Q at 2.4 GHz. The measured Q was found based on the measured 10 dB return loss bandwidth using eq.2.14. As seen, a sequential

comparison of the G/Q ratio from iteration one to the final iteration in Figure 4.27 shows that this novel method for minimizing the total occupied volume resulted in a closer approach to the optimal G/Q ratio limit. Figure 4.27 shows also the G/Q ratio for different published small antenna designs on different configurations. As seen, the final iteration provides a larger G/Q ratio than the pyramid antenna proposed in [40] and the cube antenna proposed in [44]. However, the final iteration provides a smaller G/Q ratio than the spherical antenna presented in [39] which provided very good performance due to utilizing the occupied volume to the greatest extent. Therefore, it can be concluded from this comparison that the final iteration is among the highest gain efficient small antennas.
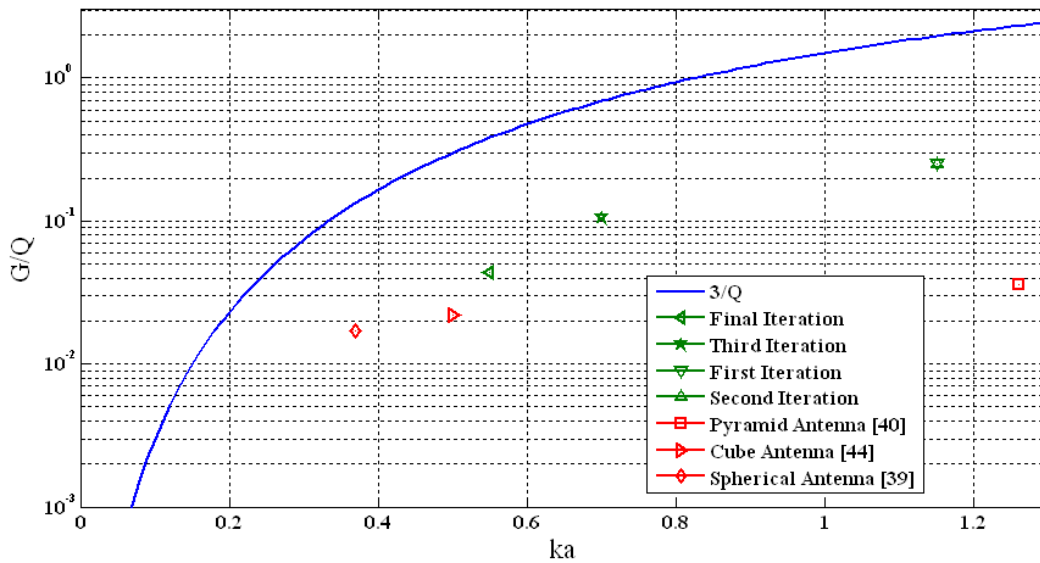


Figure 4.27: Comparison of G/Q Ratio of all the Design Iterations and Other Miniaturized Small Antennas

4.7 Conclusion

A novel method for miniaturizing dipole antennas was presented in this chapter. The method efficiently exploits the available volume. It was found that this method reduces the return loss bandwidth, and slightly reduces the antenna's gain.

An optimum design of a 3D cube antenna has been developed. Good matching response was obtained from both the simulated and measured results of this electrically small antenna. It was found that this antenna operates fine at the frequency of operation, with good radiation characteristics according to its electrical size, and it is among the highest gain efficient small antennas. Decent gain and an omni-directional pattern in the broadside direction were measured. The presented design is a good candidate to work efficiently for wireless sensor applications where the available volume is constrained.

The 3-antenna method, which was used for measuring the absolute realized gain, provided repeatable results with small uncertainty. The Wheeler Cap method that was utilized to measure the antenna efficiency provided acceptable results with low accuracy.

# CHAPTER 5

## SUMMARY AND RECOMMENDATIONS FOR FUTURE WORK

5.1 Summary

This thesis presented an insight into the design, fabrication, and testing of small antennas that are suitable for wireless sensor nodes. A review of the fundamental parameters used to characterize antennas was conducted in order to find an optimal design. As those antennas are defined as electrically small, a discussion of fundamental limitations of small antennas was presented. This discussion proved to be helpful in obtaining practical designs. It was found that small antenna measurements are challenging and prone to errors, therefore some considerations in measuring electrically small antennas were presented. Furthermore, two methods for measuring the efficiency were studied extensively and used to determine the presented designs efficiencies; the Wheeler Cap method and the gain/directivity method.

Based on the presented study of the different miniaturization techniques and the ground plane effect, the planar meandered line antenna with truncated ground plane was designed, fabricated, and tested. The study of the ground plane and testing the truncated ground plane antenna proved that the ground plane plays a fundamental role in the antenna characteristics such as: gain, bandwidth, input impedance, and resonant frequency. It was found that the truncated ground plane antenna works well at the

frequency of operation, with good radiation characteristics according to its small electrical size, however, it needed a wide ground plane to be balanced.

The study of the small antenna limitations proved that 3D antennas are preferred for applications that require efficiency concomitantly with small size. 3D antennas are also favorable for applications that require exploiting the available volume for other uses. A novel method for miniaturizing a dipole antenna was presented. This method consists of fabricating the dipole on a cube configuration. The presented 3D dipole antenna was tested, and it was found that this antenna operates fine at the frequency of operation, with good radiation characteristics according to its occupied volume. Therefore, this design is very promising in low-power sensing applications.

5.2 Recommendations

As discussed before, the final 3D dipole antenna design is more favorable for wireless sensor applications. Minimizing the overall antenna size is of concern for these applications. Therefore, more consideration can be given to minimize the occupied volume of this design. The high dielectric substrate that was selected for this design did not have a significant effect in minimizing the antenna size due to the low percentage of the radiated fields that are covered within the substrate. Minimizing the antenna size can be achieved by placing a superstrate over the dipole arms.

The antenna height is mainly restricted by the parallel plate balun length which should be $\lambda_g/4$ for optimum performance. The length of the parallel plate balun can be reduced by loading the balun with two superstrates (one from each side). Also it could be

78

interesting to study the effect of meandering the length of the parallel plate balun, and apply this approach if it will not affect the unbalanced-to-balanced transition.

Our ongoing research is to design a frequency doubling reflectenna (FDR) as the main part of the sensor node. The FDR device simply consists of receive and transmit antennas and a diode doubler as the doubling element, Figure 5.1. The device will operate by receiving a 2.4 GHz signal and re-radiating a 4.8 GHz signal. Instead of designing the two components separately, the cube configuration offers the benefit of leaving an additional space for the other components. The 4.8 GHz antenna can be fabricated on the other side of the cube; therefore minimizing the overall device volume. However, a study of integrating the 2.4 GHz antenna with the 4.8 GHz antenna should be conducted in order to determine the minimum separation distance between the antennas that is required to reduce the coupling impact. As the designed antenna is linearly polarized, the coupling effect can be minimized by setting the other antenna to be orthogonal to the first one.
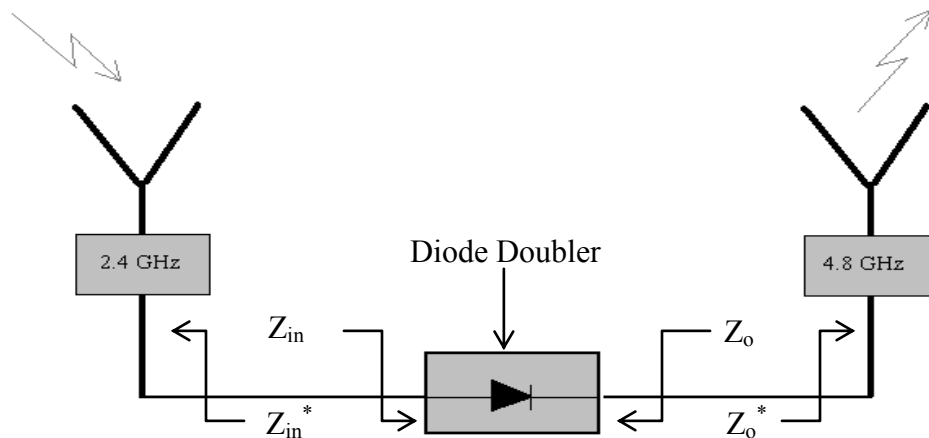


Figure 5.1: A Frequency Doubling Reflectenna Schematic with Conjugate-Matched Impedances

It was found that for improving the FDR performance the power transfer between the antennas and the diode doubler should be maximized to minimize the conversion loss [45]. The power transfer can be maximized by conjugate-matching the receive and transmit antennas to the input and output impedances of the diode doubler, Figure 5.1 (where $Z_{in}$ and $Z_{o}$ are the input and output impedances of the diode. $Z_{in}^{*}$ is the source antenna input impedance and $Z_{o}^{*}$ is the load antenna input impedance). The conjugate-match approach will decrease the bandwidth and improve the sensitivity [45].

Most of the common multiplier designs convert the input impedance of the multiplier from capacitive to inductive at the output or vice versa. One approach to achieve the conjugate-matching between the antennas and the multiplier with less matching circuits is by designing the antennas to operate off-resonance. As the designed antenna impedance variation over frequency is similar to the conventional dipole antenna, one antenna can be designed to operate at $f_{o}$ + delta and the other antenna at $f_{o}$ − delta, Figure 5.2. The parallel plate balun width and the matching line are also helpful in designing for specific input impedances; therefore the number of the matching networks components may be reduced.
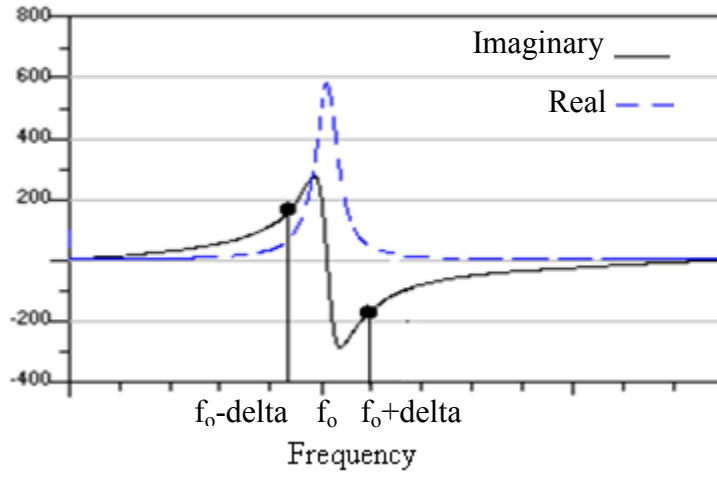
Figure 5.2: Impedance Variation over Frequency for Conventional Dipole

# REFERENCES

[1] Whyte, G, "An Omnidirectiona, Low Cost, Low Profile, 2.45 GHz Microstrip Fed Rectaxial Antenna for Wirelss Sensor Network Applications" IEE and IEEE conference, Loughborough Antennas and Propagation Conference, LAPC 2006.

[2] E. Kranakis, D. Krizanc, and E. Williams, "Directional versus Omnidirectional Antennas for Energy Consumption and k-Connectivity of Networks of Sensors," in OPODIS 2004, pp. 357-368, 2004.

[3] Rolfsnes, H.O.; Maccarini, P.F.; Jacobsen, S.; Stauffer, P.R.; , "Design of spiral antennas for radiometric temperature measurement," Engineering in Medicine and Biology Society, 2004. IEMBS '04. 26th Annual International Conference of the IEEE, vol.1, no., pp.2522-2525, 1-5 Sept. 2004

[4] H.A. Wheeler, "The Radiansphere around a Small Antenna," Proceedings of the IRE , vol.47, no.8, pp.1325-1331, Aug. 1959

[5] Miron, Douglas B, "Small antenna design", Newnes/Elesevier, Burlington, MA, PP.235-246, 2006

[6] Fawaz T. Ulaby, "Fundamental of Applied Electromagnetics", Pearson Education, NJ, PP.372-390, 2007

[7] C.A. Balanis, "Antenna Theory", New York: John Wiley & Sons, 2nd ed., PP.28-98,865-871,1997

[8] Pozar, D.M.; Kaufman, B, 'Comparison of Three Methods for the Measurement of Printed Antenna Efficiency' IEEE Antennas and Propagation Magazine, Volume.36, pp.136-139, Jan 1988

[9] Wheeler, H.A.; , "Fundamental Limitations of Small Antennas," Proceedings of the IRE , vol.35, no.12, pp. 1479- 1484, Dec. 1947

[10] H. Wheeler, "Small antennas," IEEE Transactions on Antennas and Propagation, vol.23, no.4, pp.462-469, Jul. 1975

[11] L.J. Chu, "Physical Limitation of Omni-Directional Antennas," Journal of Applied Physics, vol. 19, pp.1163-1175, Dec. 1948

[12] J. S. McLean, "A re-examination of the fundamental limits on the radiation Q of electrically small antennas," IEEE Transactions on Antennas and Propagation, vol.44, no.5, pp.672-676, May 1996

[13] R.C. Hansen, "Fundamental limitations in antennas," Proceedings of the IEEE, vol.69, no.2, pp.170-182, Feb. 1981

[14] R. F. Harrington, "Effect of antenna size on gain, bandwidth and efficiency", J. Res. Nat. Bur. Stand., vol.64-D, pp.1-12, Jan./Feb. 1960

[15] J.C.-E. Sten, A. Hujanen, P.K. Koivisto, "Quality factor of an electrically small antenna radiating close to a conducting plane," IEEE Transactions on Antennas and Propagation, vol.49, no.5, pp.829-837, May 2001

[16] Randy Bancroft, "Fundamental Dimension Limits of Antennas Ensuring Proper Antenna Dimensions in Mobile Device Designs", Centurion Wireless Technologies Westminster, Colorado.

[17] S.R. Best, "A discussion on the quality factor of impedance matched electrically small wire antennas," IEEE Transactions on Antennas and Propagation, vol.53, no.1, pp.502-508, Jan. 2005

[18] A. K. Skrivervik, J. F. Zurcher, O. Staub, J.R. Mosig, "PCS antenna design: the challenge of miniaturization," IEEE Antennas and Propagation Magazine, vol.43, no.4, pp.12-27, Aug 2001

[19] Kildal, P.-S.; Best, S.R, "Further investigations of fundamental directivity limitations of small antennas with and without ground planes," Antennas and Propagation Society International Symposium, 2008. AP-S 2008. IEEE, vol., no., pp.1-4, 5-11 July 2008

[20] John L. Volakis, Chi-Chih Chin, Kyohei Fujimoto, "Small Antennas: Miniaturization Techniques & Applications", The McGraw-Hill, PP.1-100, 2010

[21] Bernhard, J.T.; Adams, J.J.; Anderson, M.D.; Martin, J.M.; , "Measuring electrically small antennas: Details and implications," Antenna Technology, 2009. iWAT 2009. IEEE International Workshop on , vol., no., pp.1-4, 2-4 March 2009

[22] Collins, B.S.; Saario, S.A.; , "The use of baluns for measurements on antennas mounted on small groundplanes," Antenna Technology: Small Antennas and Novel Metamaterials, 2005. IWAT 2005. IEEE International Workshop on , vol., no., pp. 266- 269, 7-9 March 2005

[23] C. Icheln, J. Krogerus, and P. Vainikainen, "Use of balun chokes in small-antenna radiation measurements," IEEE Trans. on Instrumentation and Measurement, vol. 53, no. 2, pp. 498-506, April 2004.

[24] T. H. Loh and M. Alexander, "New facility for minimally invasive measurements of electrically small antennas," in Proc. Loughborough Antennas and Propagation Conf., pp. 313-316, 2008.

[25] Hosung Choo; Rogers, R.; Hao Ling, 'On the Wheeler Cap Measurement of the Efficiency of Microstrip Antennas' IEEE Antennas and Propagation Magazine, Volume.53, pp.2328-2332, July 2005

[26] Higashi, E.; Iida, Y.; Omura, Y, "A Study of Antenna Efficiency Measurements by Wheeler Cap Method Applied to Planer Inverted-F Antenna (PIFA)" Signals, Systems and Electronics, 2007. ISSSE '07. International Symposium, Volume.53, pp.599-601, Aug 2007

[27] Newman, E.; Bohley, P.; Walter, C.; , "Two methods for the measurement of antenna efficiency," Antennas and Propagation, IEEE Transactions on , vol.23, no.4, pp. 457- 461, Jul 1975

[28] O. Staub, J.-F. Zürcher, A. Skrivervik" Some considerations on the correct measurement of the gain and bandwidth of electrically small antennas" Microwave and Optical Technology Letters, vol.17, no 3,pp156-160, 1998

[29] Soontornpipit, P.; Furse, C.M.; You Chung Chung; "Design of implantable microstrip antenna for communication with medical implants," Microwave Theory and Techniques, IEEE Transactions on , vol.52, no.8, pp. 1944- 1951, Aug. 2004

[30] Delaveaud, C.; Sufyar, S.;"A miniaturization technique of a compact omnidirectional antenna," Antennas and Propagation, 2009. EuCAP 2009. 3rd European Conference on , vol., no., pp.384-388, 23-27 March 2009

[31] R. Garg, P. Bhartia, I. Bahl and A. Ittipiboon, "Microstrip Antenna Design Handbook", Artech House: Norwood, MA, PP.1-657, 2001

[32] Zurcher, J.-F.; Skrivewik, A.K.; Staub, O.; , "SMILA: a miniaturized antenna for PCS applications," Antennas and Propagation Society International Symposium, 2000. IEEE , vol.3, no., pp.1646-1649 vol.3, 2000

[33] Best, S.R.; Hanna, D.L.; , "A Performance Comparison of Fundamental Small-Antenna Designs," Antennas and Propagation Magazine, IEEE , vol.52, no.1, pp.47-70, Feb. 2010

[34] Huynh, M.-C.; Stutzman, W.; , "Ground plane effects on planar inverted-F antenna (PIFA) performance," Microwaves, Antennas and Propagation, IEE Proceedings - , vol.150, no.4, pp. 209- 213, 8 Aug. 2003

[35] Salonen, P.; , "Effect of groundplane size on radiation efficiency and bandwidth of dual-band U-PIFA," Antennas and Propagation Society International Symposium, 2003. IEEE , vol.3, no., pp. 70- 73 vol.3, 22-27 June 2003

[36] Horng-Dean Chen; "Compact Broadband Microstrip-Line-Fed Sleeve Monopole Antenna for DTV Application and Ground Plane Effect," Antennas and Wireless Propagation Letters, IEEE, vol.7, no., pp.497-500, 2008

[37] Best, S.R.; , "The Significance of Ground-Plane Size and Antenna Location in Establishing the Performance of Ground-Plane-Dependent Antennas," Antennas and Propagation Magazine, IEEE , vol.51, no.6, pp.29-43, Dec. 2009

[38] Tsachtsiris, G.; Soras, C.; Karaboikis, M.; Makios, V.; "Ground plane effect on the performance of a printed Minkowski monopole antenna," Applied Electromagnetics and Communications, 2003. ICECom 2003. 17th International Conference on , vol., no., pp. 197- 200, 1-3 Oct. 2003

[39] Best, S.R.; , "Low Q electrically small linear and elliptical polarized spherical dipole antennas," Antennas and Propagation, IEEE Transactions on , vol.53, no.3, pp. 1047- 1053, March 2005

[40] Melais, S., et al., "Origami packaging – novel printed antenna technology for ad-hoc sensor applications," 40th International Symposium on Microelectronics, Oct 2007.

[41] Thomas A. Milligan, "Modern Antenna Design", Second Edition, John Wiley& Sons, Inc., New jersey, PP.218-260, 2005

[42] David M. Pozar, "Microwave Engineering", Third Edition, John Wiley & Sons, Inc., new Jersey, PP.98-106, 1998

[43] T. Vasiliadis, E. Vaitsopoulos, and G. Sergiadis, "A wideband printed bipole antenna with optimized tapered feeding balun for ISM and FW bands", Microwave Opt Technol Lett 43, 437–441, 2004.

[44] Kruesi, C.M.; Vyas, R.J.; Tentzeris, M.M.; , "Design and Development of a Novel 3-D Cubic Antenna for Wireless Sensor Networks (WSNs) and RFID Applications," Antennas and Propagation, IEEE Transactions on , vol.57, no.10, pp.3293-3299, Oct. 2009

[45] Presas, S.M.; Weller, T.M.; Silverman, S.; Rakijas, M.; , "High efficiency diode doubler with conjugate- matched antennas," Microwave Conference, 2007. European , vol., no., pp.250-253, 9-12 Oct. 2007